
VertiBench: Advancing Feature Distribution Diversity in Vertical Federated Learning Benchmarks

Zhaomin Wu, Junyi Hou, Bingsheng He
 Department of Computer Science
 National University of Singapore
 {zhaomin, junyi.h, hebs}@comp.nus.edu.sg

Abstract

Vertical Federated Learning (VFL) is a crucial paradigm for training machine learning models on feature-partitioned, distributed data. However, due to privacy restrictions, few public real-world VFL datasets exist for algorithm evaluation, and these represent a limited array of feature distributions. Existing benchmarks often resort to synthetic datasets, derived from arbitrary feature splits from a global set, which only capture a subset of feature distributions, leading to inadequate algorithm performance assessment. This paper addresses these shortcomings by introducing two key factors affecting VFL performance - feature importance and feature correlation - and proposing associated evaluation metrics and dataset splitting methods. Additionally, we introduce a real VFL dataset to address the deficit in image-image VFL scenarios. Our comprehensive evaluation of cutting-edge VFL algorithms provides valuable insights for future research in the field.

1 Introduction

The increasing demand for ample, high-quality data for training advanced machine learning models is evident, particularly in the context of large language models [1]. However, real data, often sensitive and distributed across multiple parties, presents a challenge, especially in the face of strict privacy regulations like the GDPR [2]. As a result, federated learning [3] has been highlighted as a promising approach to train machine learning models on distributed data while ensuring privacy. In this study, we consider a broad definition of federated learning [4], encompassing all privacy-preserving collaborative learning paradigms, including assisted learning [5, 6] and split learning [7, 8]. Given the emerging variety of federated learning approaches [4, 9, 10], the importance of comprehensive benchmarks for evaluating these new algorithms is underscored.

The landscape of federated learning benchmarks, featuring contributions such as FedScale [11], MNIST [12], FedEval [13], and NIID-Bench [14], predominantly caters to horizontal federated learning (HFL), wherein each party possesses a subset of instances. In comparison, vertical federated learning (VFL) - where each party holds a subset of features - is notably under-addressed.

The development of real-world VFL benchmarks faces two main hurdles. First, privacy concerns inherent to federated learning inhibit the public sharing of distributed data. Second, the current limited pool of actual VFL datasets, such as those in the OARF benchmark [15], NUS-WIDE [16], and Vehicle [17], may not sufficiently represent the broad range of possible VFL scenarios (Figure 2c; Section 5). This scarcity and underrepresentation highlight the urgent need for synthetic VFL benchmarks that can facilitate a comprehensive evaluation of VFL algorithms across diverse scenarios.

Existing efforts to construct synthetic VFL benchmarks have struggled to represent the diversity of real-world scenarios. Benchmarks such as OARF [15], FedML [18], and LEAF [19] fabricate vertically partitioned data by randomly assigning an equal number of features to synthetic parties.

Some studies [5, 20, 21] resort to a simplistic approach, manually dividing features without offering a substantial rationale for their choice. Furthermore, these existing benchmarks [15, 18, 19] do not offer a meaningful comparison of cutting-edge VFL algorithms. Hence, it becomes crucial to critically examine the key factors influencing VFL algorithm performance, and thoughtfully design synthetic VFL benchmarks that reflect these considerations.

The task of creating a systematic synthetic VFL benchmark hinges on identifying key factors influencing VFL algorithm performance. Current synthetic benchmarks for non-i.i.d. HFL like NIID-Bench [14] are inapplicable to VFL their assumptions about feature space and instance equality. In particular, HFL benchmarks assume that all parties operate within the same feature space, a presumption that doesn't conform to VFL's distributed feature scenario. Moreover, the instance equality presupposed by NIID-Bench during allocation doesn't apply when dealing with features of varied importance, underscoring the unique challenges in the analysis of synthetic VFL benchmark.

Given these limitations, our study conducts a systematic analysis to identify feature importance and correlation as two crucial determinants of VFL performance. Accordingly, we propose *VertiBench*, a comprehensive VFL benchmark which introduces novel feature-splitting methods for synthetic dataset generation and a new real-world VFL dataset. Our key contributions include: (1) We develop new feature-splitting methods that generate synthetic datasets based on feature importance and correlation, covering a diverse range of VFL scenarios. (2) We introduce a real-world VFL dataset, filling a noted gap in image-image VFL scenarios. (3) We devise methods to quantify the importance and correlation of real-world VFL datasets, allowing them to align with our synthetic datasets. (4) We conduct rigorous benchmarks of advanced VFL algorithms across diverse scenarios, thereby offering valuable insights for future research. For example, we demonstrate the scalability of certain VFL algorithms, challenging prior assumptions about VFL scaling difficulties [15], and emphasize the importance of communication efficiency in VFL, especially for imbalanced distributed datasets.

2 Related Work

Vertical federated learning datasets. The scarcity and limited range of real-world VFL datasets [15, 16, 17] in benchmarks and studies [18, 19] underscore the need for synthetic VFL datasets capable of depicting a broader spectrum of scenarios. Given VFL's focus on data privacy, obtaining such real datasets is challenging. Synthetic benchmarks [18, 19] and VFL study datasets [5, 7, 22] commonly rely on unexplained random or manual feature splitting, which often represents scenarios of balanced feature importance and high inter-party correlation (Figure 1, 2c). This situation indicates a pressing demand for systematic methods to generate synthetic VFL datasets that accurately reflect a diverse set of scenarios, fostering comprehensive evaluation of VFL algorithms.

Feature importance. The Shapley value [23, 24, 25], used to assess party contributions in federated learning [26, 27, 28], has significant computational costs, rendering it unsuitable for guiding feature splitting. Certain methodologies [14, 29] utilize a Dirichlet distribution for global dataset random split, creating imbalanced federated learning datasets. However, they do not consider the partitioning of features of varying importance.

Feature correlation. The task of efficiently gauging correlation among two groups of features is challenging despite well-studied individual feature correlation [30, 31]. The Shapley-Taylor index, proposed for evaluating correlation between feature sets [32], is computationally intensive (NP-hard), and unsuitable for high-dimensional datasets. The determinant of the correlation matrix [33] efficiently estimates inter-party correlation but is over-sensitive to linearly correlated features, impeding its use in feature partitioning. A more refined metric - the multi-way correlation coefficient (mcor) [34], addresses this, but like the determinant, it struggles with unequal feature numbers across parties, a typical VFL scenario, due to the assumption of a square correlation matrix.

3 VFL Algorithms

This section critically reviews current VFL algorithms, with a focus on accuracy, efficiency, and communication size. *VertiBench* concentrates on standard supervised learning tasks such as classification and regression within synchronized parties, summarized in Table 1. Notably, this benchmark excludes studies exploring different VFL aspects such as privacy [35], fairness [36], data pricing [37], asynchronization [20, 38, 39], latency [40], and other tasks like unsupervised learning [41], matrix

factorization [42], multi-task learning [8], and coreset construction [43]. While most VFL algorithms presume accurate inter-party data linking, we adopt this approach in VertiBench, despite recent contrary findings [44, 45] that this assumption may not be true. We refer to parties with and without labels as *primary* and *secondary parties* respectively.

Table 1: Summary of existing VFL algorithms

Category	Model ¹	Algorithm	Contribution ²	Code ³	Data ⁴	Split ⁵
Ensemble-based	Any	AL [6]	Accuracy	[46]	Syn	Manual
		GAL [5]	Accuracy	[47]	Syn	Manual
Split-based	NN	SplitNN [7]	Accuracy	[48]	Syn	N/A
		C-VFL [21]	Communication	[49]	Syn	Manual
		BlindFL [50]	Efficiency	N/A	Syn	Manual
	GBDT	SecureBoost [22]	Accuracy	[51]	Syn	Manual
		Pivot [52]	Accuracy	[53]	Syn	Manual
		FedTree [29]	Accuracy, Efficiency	[54]	Syn	Random
		VF2Boost [55]	Efficiency	N/A	Syn	Manual

¹ Abbreviations: NN - neural network; GBDT - gradient boosting decision trees; Any - model-agnostic.

² Privacy is not evaluated in VertiBench, and therefore omitted, despite being a contribution of some studies.

³ Code availability: N/A - code not publicly accessible due to commercial issues.

⁴ Dataset in experiments: Syn - synthetic datasets partitioned from global datasets.

⁵ Datasets used in the experiments: Manual - features manually split without specific reasons; Random - features randomly split without explanation; N/A - no VFL experiments conducted.

The existing methods can be bifurcated into two categories: *ensemble-based* and *split-based*. The distinguishing factor lies in the independent prediction capability of each party. Ensemble-based methods involve parties each maintaining a full model for local feature prediction, with collaborative ensemble methods during training, while split-based methods require each party to hold a partial model forming different inference stages of the full model. Consequently, split-based partial models cannot perform independent inference. For split-based models, our focus is on advanced models such as neural networks (NNs) and gradient boosting decision trees (GBDTs) [56], though VertiBench can accommodate various models [57, 58]. Split-NN-based models are trained by transferring representations and gradients, while split-GBDT-models are trained by transferring gradients and histograms. A more detailed comparison of ensemble-based and split-based algorithms is provided in Appendix B.

4 Synthetic VFL Datasets

4.1 Factors that affect VFL performance

Suppose there are K parties. Denote the data on party P_k as a random vector \mathbf{X}_k ($1 \leq k \leq K$). Denote the label as a random variable y . A supervised learning algorithm maximizes the likelihood function where hypothesis h represents models and parameters, i.e., $L(y|\mathbf{X}_K, \dots, \mathbf{X}_1; h)$.

These supervised learning algorithms estimate the following probability mass function. The proof of Proposition 1 is provided in Appendix A.

Proposition 1. *The probability mass function can be written as*

$$\log \mathcal{P}(y|\mathbf{X}_K, \dots, \mathbf{X}_1) = \sum_{i=1}^K \log \frac{\mathcal{P}(y|\mathbf{X}_k, \dots, \mathbf{X}_1)}{\mathcal{P}(y|\mathbf{X}_{k-1}, \dots, \mathbf{X}_1)} + \log \mathcal{P}(y) \quad (1)$$

In VFL, $\mathcal{P}(y)$ is the same for all the parties. The skewness among K parties is determined by K ratios of distributions. Interestingly, this ratio quantifies the divergence between two marginal probability distributions of y - one inclusive of \mathbf{X}_k and the other exclusive of \mathbf{X}_k . Essentially, the ratio estimates the impact on the global distribution when the features of a single party are excluded. This can be interpreted as the **importance** of a given party.

It is important to note that Proposition 1 is applicable regardless of the order of $\mathbf{X}_1, \dots, \mathbf{X}_k$. For a more precise evaluation of each party's importance, especially considering the independence among

features, Shapley value has proven to be a useful measure. It has been employed to estimate the importance of each party in vertical federated learning scenarios [26, 28].

In another aspect, the ratio $\frac{\mathcal{P}(y|\mathbf{X}_k, \dots, \mathbf{X}_1)}{\mathcal{P}(y|\mathbf{X}_{k-1}, \dots, \mathbf{X}_1)}$ is determined by the **correlation** between \mathbf{X}_k and $\mathbf{X}_1, \dots, \mathbf{X}_{k-1}$. In other words, the global distribution is affected by the feature correlation between different parties.

In summary, we highlight feature importance and correlation as two crucial factors that could potentially influence the performance of VFL algorithms. We treat importance and correlation as independent variables affecting $\frac{\mathcal{P}(y|\mathbf{X}_k, \dots, \mathbf{X}_1)}{\mathcal{P}(y|\mathbf{X}_{k-1}, \dots, \mathbf{X}_1)}$ in our analysis, despite a potential innate correlation between the two. The subsequent sections will introduce our approach to generating synthetic datasets based by these two factors.

4.2 Feature Importance

In light of the computational expense incurred by the Shapley value method, an alternative and more efficient strategy is necessary to perform feature splits based on importance. With all parties exhibiting symmetry in the context of \mathbf{X} , varying the importance among parties essentially translates to varying the variance of the importance among them. Assuming each party P_i possesses an importance factor $\alpha_i > 0$, we propose the implementation of the Dirichlet distribution parameterized by $\{\alpha_i\}_{i=1}^K$ for feature splitting. This approach ensures two beneficial properties post-split: (1) a larger α_i guarantees a higher expected importance for P_i , and (2) a smaller $\|\{\alpha_i\}_{i=1}^K\|_2$ assures a greater variance in the importance among parties.

More specifically, we propose a feature splitting method based on feature importance. After initializing local datasets for each party, a series of probabilities p_1, \dots, p_K s.t. $\sum_{i=1}^K p_i = 1$ is sampled from a Dirichlet distribution $\text{Dir}(\alpha_1, \dots, \alpha_K)$. Each feature is randomly allocated to a party P_k , selected based on the probabilities p_k . To accommodate algorithms that fail when faced with empty features, we can ensure each party is initially provided with a random feature before the algorithm is set in motion. Detailed formalization of this algorithm can be found in Appendix C.

Theorem 1. *Consider a feature index set $\mathcal{A} = \{1, 2, \dots, m\}$ and a characteristic function $v : 2^{\mathcal{A}} \rightarrow \mathbb{R}$ such that $v(\emptyset) = 0$. Let $\phi_j(v)$ denote the importance of the j -th feature on v such that $\sum_{j=1}^m \phi(j) = v(\mathcal{A})$. Assume that the indices in \mathcal{A} are randomly distributed to K parties with probabilities r_1, \dots, r_K where $\sum_{i=1}^K r_i = 1$. Given budgets $b_i = r_i v(\mathcal{A})$, let Z_i be the sum of feature importance for party i . Then, we have $\forall i \in [1, K], \mathbf{E}[Z_i] = b_i$ and $\mathbf{E}[Z_i] \propto r_i$.*

The proof of Theorem 1 is provided in Appendix A. The metric of importance, $\phi_j(v)$, comprises the Shapley value and the recently proposed Shapley-CMI [28]. We assert in Theorem 1 that the expected cumulative importance of each party is proportional to the ratio generated by the Dirichlet distribution. The inherent properties of the Dirichlet distribution ensure that: (1) a larger value of α_i leads to a higher expected value of r_i , and (2) a smaller value of $\|\{\alpha_i\}_{i=1}^K\|_2$ results in a larger variance in r_i . Hence, the proposed method naturally aligns with the requirements for feature importance.

4.3 Feature Correlation

In the initial stages of our investigation into feature-split methods based on correlation, we first look at the evaluation of feature correlation. Building upon established methods that utilize a metric grounded in correlation matrices [33, 34], we propose a novel metric to examine the correlation when the parties involved possess unequal numbers of features. Our approach hinges on the use of the standard variance of the singular values of the correlation matrix. This serves as an efficient measure of the overall correlation between two parties. Since the feature-wise correlation is an orthogonal research area, we selected Spearman rank correlation [59] due to its capability to handle non-linear correlation.

To elaborate further, we denote the column-wise correlation matrix between two matrices, \mathbf{X}_i and \mathbf{X}_j , as $\text{cor}(\mathbf{X}_i, \mathbf{X}_j)$. As a result, we formally define the correlation between two entities, $\mathbf{X}_i \in \mathbb{R}^{n \times m_i}$

and $\mathbf{X}_j \in \mathbb{R}^{n \times m_j}$, in terms of their respective parties as Equation 2.

$$\text{Pcor}(\mathbf{X}_i, \mathbf{X}_j) := \frac{1}{d} \sqrt{\sum_{i=1}^d (\sigma_i(\text{cor}(\mathbf{X}_i, \mathbf{X}_j)) - \bar{\sigma})^2}, \quad d = \min(m_i, m_j) \quad (2)$$

In this equation, $\sigma_i(\cdot)$ means the i -th singular value of a matrix, while $\bar{\sigma}$ stands for their mean value.

$$\text{Icor}(\mathbf{X}_1, \dots, \mathbf{X}_K) := \frac{1}{K(K-1)} \sum_{i=1}^K \sum_{j=1, j \neq i}^K \text{Pcor}(\mathbf{X}_i, \mathbf{X}_j) \quad (3)$$

This correlation-based feature-split algorithm, as depicted in Algorithm 1, is meticulously designed to allocate features across multiple parties while taking into account the correlations inherent among the features. The algorithm’s operation is premised on the provision of a defined number of features for each party, represented as m_1, \dots, m_K . Commencing with the initialization of a column permutation matrix, denoted as \mathbf{P} , to an identity matrix (line 1), the algorithm proceeds to define a score function, $f(\mathbf{P}; \mathbf{X})$, which represents the overall correlation Icor after the features have undergone permutation by \mathbf{P} (line 2). Subsequently, the algorithm determines the lower and upper bound of the score function (lines 3-4). This forms the basis for calculating the target correlation $f^*(\mathbf{X}; \beta)$, which is a linear interpolation between the lower and upper bounds controlled by the correlation index β (line 5). Next, the algorithm locates the optimal permutation matrix \mathbf{P}^* by solving a permutation-based optimization problem. Notably, we employ the Biased Random-Key Genetic Algorithm (BRKGA) [60] for this purpose. The final step of the algorithm splits the features according to the derived optimal permutation and the pre-set number of features for each party (lines 6-7).

Algorithm 1: Feature Splitting by Correlation

Input: Global dataset $\mathbf{X} \in \mathbb{R}^{n \times m}$, correlation index β , number of features m_1, \dots, m_K

Output: Local datasets $\mathbf{X}_1, \dots, \mathbf{X}_K$

```

1  $\mathbf{P} \leftarrow \mathbf{I}$ ; /* Initiate permutation matrix */
2  $f(\mathbf{P}; \mathbf{X}) := \text{Icor}(\mathbf{X}_1^P, \dots, \mathbf{X}_K^P)$  s.t.  $\mathbf{X}_1^P, \dots, \mathbf{X}_K^P \leftarrow$  split features of  $\mathbf{X}\mathbf{P}$  by  $m_1, \dots, m_K$ ;
3  $f_{\min}(\mathbf{X}) = \min_{\mathbf{P}} f(\mathbf{P}; \mathbf{X})$ ; /* Calculate lower bound */
4  $f_{\max}(\mathbf{X}) = \max_{\mathbf{P}} f(\mathbf{P}; \mathbf{X})$ ; /* Calculate upper bound */
5  $f^*(\mathbf{X}; \beta) \leftarrow (1 - \beta)f_{\min}(\mathbf{X}) + \beta f_{\max}(\mathbf{X})$ ; /* Calculate target correlation */
6  $\mathbf{P}^* \leftarrow \arg \min_{\mathbf{P}} |f(\mathbf{P}; \mathbf{X}) - f^*(\mathbf{X}; \beta)|$ ; /* Find the permutation matrix */
7  $\mathbf{X}_1^P, \dots, \mathbf{X}_K^P \leftarrow$  split features of  $\mathbf{X}\mathbf{P}^*$  by  $m_1, \dots, m_K$ ;
8 return  $\mathbf{X}_1, \dots, \mathbf{X}_K$ 

```

Owing to the fact that the optimization approach requires many invocations of Icor, it is important that this process is conducted with the highest degree of efficiency. For datasets of smaller dimensions, singular values can be directly computed utilizing Singular Value Decomposition (SVD) [61]. However, in the case of high-dimensional datasets, we resort to employing Truncated SVD [62] to estimate the largest top- d_t singular values, with the remaining singular values assumed as zero prior to calculating the standard variance. It is worth noting that we make use of GPU acceleration to expedite the computation of Icor, thereby ensuring that the optimization procedure is as swift and efficient as possible. Our experiments, as presented in Appendix D, validate that both split methods can complete within a reasonable time.

Empirical Validation. We conduct extensive experiments to rigorously evaluate the practical performance of our proposed correlation evaluation metric and the correlation-based feature-split algorithm; the details are in Appendix D. Briefly, for the correlation evaluation metric Icor, we observe that Pcor mirrors the behavior of mcor [34] in assessing inner-party correlation and displays a similar trend to mcor for inter-party correlation evaluation. Moreover, we split features of synthetic datasets of different β values using Algorithm 1, contrasting it with a random split. The absolute correlation matrix visualized in Figure 1 suggests that as β increases, so does inter-party correlation. In contrast, random feature splitting does not effectively portray scenarios with low inter-party correlation.

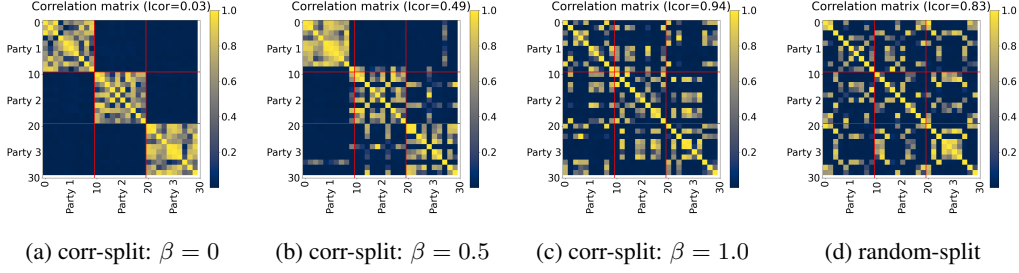


Figure 1: Absolute correlation matrix of the global dataset with party boundaries indicated by red lines. Icor means inter-party correlation. (a),(b),(c) - correlation-based split; (d) random split.

5 Real-world VFL Datasets

Real-world VFL datasets, though highly desirable, are limited in scope and type, often encompassing tabular-tabular data, as in Vehicle [17], MovieLens [15], Songs [15], and tabular-image data, as in NUS-WIDE [16]. Notably missing are image-image datasets. Addressing this, we introduce a real-world VFL dataset, *Satellite*, adapted from [63], containing 62,832 images across 16 parties, simulating a practical VFL scenario of collaborative location identification via multiple satellites. Further details on Satellite’s construction are in Appendix E.

An in-depth analysis of the Satellite dataset, using our proposed metrics and the visualization of absolute correlation matrix (Figure 2b), reveals low inter-party correlation (Icor) and high inner-party correlation, similar to NUS-WIDE (Figure 2a). These results underscore the fact that random feature splits, which usually result in larger β values (Figures 1d and 2c), may not truly represent real-world scenarios, reinforcing the need for systematic VFL datasets generation methods.

Estimating α and β for real VFL datasets. In order to align real datasets with the synthetic ones generated by VertiBench, we put forward methods to estimate α and β for real VFL datasets.

To calculate α , we determine the significance of each party by adding up the Shapley value of its features. We do this efficiently by estimating Shapley values on a select subset. These Shapley values are then normalized and treated as Dirichlet parameters α_i for each party P_i , in line with Theorem 1. To approximate the scale of the Dirichlet parameters and align them with the generation of synthetic datasets, we find a symmetric Dirichlet distribution $\text{Dir}(\bar{\alpha})$ that has the same variance as $\text{Dir}(\alpha_1, \dots, \alpha_K)$, as given in Proposition 2. This value of $\bar{\alpha}$ reflects the variance in feature importance across parties. The proof is provided in Appendix A.

Proposition 2. *Given a Dirichlet distribution $\text{Dir}(\alpha_1, \dots, \alpha_K)$ with mean variance σ , symmetric Dirichlet distribution $\text{Dir}(\bar{\alpha})$ that has the same mean variance σ if $\bar{\alpha} = \frac{K-1-K^2\sigma}{K^3\sigma}$.*

To estimate β , we start by computing the potential minimum and maximum values of Icor by shuffling the features among parties, denoted as Icor_{\min} , Icor_{\max} . Next, we estimate the Icor of the actual dataset, $\text{Icor}_{\text{real}}$, and derive the β value using $\beta = \min \left\{ \max \left\{ \frac{\text{Icor}_{\text{real}} - \text{Icor}_{\min}}{\text{Icor}_{\max} - \text{Icor}_{\min}}, 0 \right\}, 1 \right\}$. It is important to note that in real-world scenarios, $\text{Icor}_{\text{real}}$ might fall slightly outside the range of Icor_{\min} , Icor_{\max} due to the constraints of optimization algorithms. To rectify this, we clip the estimated β to ensure $\beta \in [0, 1]$.

Using the estimated α and β , we display the importance and correlation of existing real datasets within the VertiBench-supported range in Figure 2c. We note that real datasets represent a limited set of VFL scenarios with a large α and small β , indicating a high degree of feature imbalance and low inter-party correlation. Further, conducting random feature splits, as is common in existing VFL experiments, results in a distinct extreme characterized by high values of both α and β . This observation underscores the importance of VertiBench, which can generate a broad range of VFL scenarios for robust evaluation of VFL algorithms.

6 Experiment

This section comprehensively benchmarks cutting-edge VFL algorithms. The experimental settings are delineated in Section 6.1, with results for VFL accuracy and communication efficiency presented

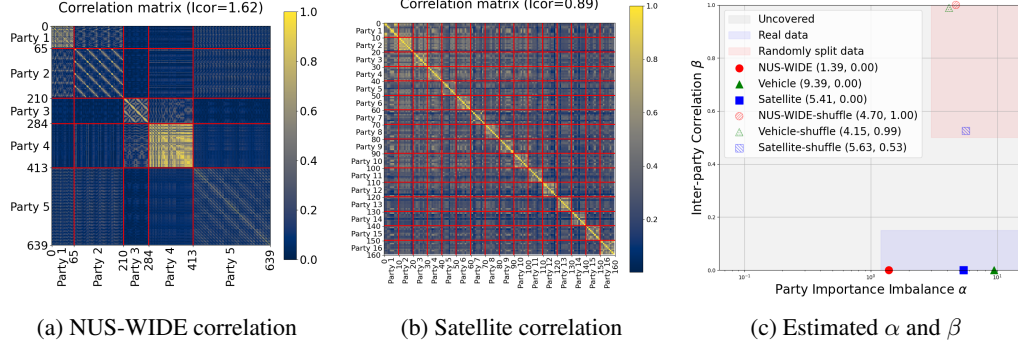


Figure 2: (a), (b) Matrix of feature absolute correlation with party boundaries marked in red; (c) scope coverage of real and randomly split datasets in terms of feature importance and correlation.

in Sections 6.2 and 6.3, respectively. Additional evaluations, including scalability, training time, and performance on real datasets, are discussed in Appendix G. Each experiment elucidates results and provides relevant insights, highlighting (1) the performance-communication tradeoff of NN-based and boosting-based methods, (2) the necessity for advanced communication-efficient algorithms for imbalanced distributed datasets, and (3) the scalability potential of VFL algorithms.

6.1 Experimental Settings

This subsection includes the datasets, evaluated algorithms, and training methodology. Detailed dataset specifications, environments, and hyperparameter settings can be found in Appendix F.

Datasets. Our experimental design incorporates seven public datasets, namely covtype [64], msd [65], gisette [66], realsim [67], epsilon [68], letter [69], and radar [70], detailed in Appendix F. The msd dataset is used for regression tasks, while the others cater to classification tasks. Each dataset is partitioned into 80% training and 20% testing instances. The datasets’ features are distributed among multiple parties (typically four), split based on feature importance (α) or correlation (β). In the correlation-based split, each party is assigned an equal number of dataset features.

Algorithms. We assess extensive code-available VFL algorithms in our experiments, including split-NN-based (SplitNN [7], C-VFL [21]), split-GBDT-based (FedTree [29], SecureBoost [22], Pivot [52]), and ensemble-based (GAL [5]) algorithms. AL [6] is excluded due to its inferiority to GAL [5]. For fairness, experiments are conducted without encryption or noise addition. In light of the reported minor variations in accuracy and communication (w/o encryption) among split-GBDT-based methods like FedTree, SecureBoost, and Pivot due to precision issues [22, 52], we have elected to use FedTree as a representative in our evaluation of their performance and communication costs.

Training. For classification tasks, we use accuracy as the evaluation metric, while regression tasks are evaluated using the Root Mean Square Error (RMSE). To ensure the reliability of our results, we conduct five runs for each algorithm, using seeds ranging from 0 to 4 to randomly split the datasets for each run, and then compute their mean metrics and standard deviation. Detailed hyper-parameter settings for each algorithms are provided in Appendix F.

6.2 VFL Accuracy

In this subsection, we study the performance of VFL algorithms by varying the data split parameters, α and β , and assessing the resulting impact on the accuracy. Our analysis includes a range of algorithm types, namely split-NN-based, split-GBDT-based, and ensemble-based methods. The performance is detailed in Table 2. From our exploration, we can draw three key observations.

The influence of split parameters α and β on VFL performance varies significantly with the choice of algorithm and dataset. The performance of certain algorithms, such as SplitNN and FedTree, remains relatively consistent across different α and β values. For others, notably C-VFL, these parameter changes can cause substantial variations in performance. For instance, on the epsilon dataset, C-VFL’s accuracy fluctuates by up to 12% and 10% when α and β are adjusted from 0.1 to 100 and from 0 to 1.0, respectively. Despite the potential significant influence of α and β parameters,

their effect on accuracy seems to be contingent upon specific dataset-algorithm combinations. This underlines the importance of extensive evaluations across a broader spectrum of α and β values, a critical step towards illustrating the robustness of VFL algorithms.

SplitNN often leads in accuracy across most datasets; however, the performance of split-GBDT-based and ensemble-based methods can vary significantly depending on the dataset. As anticipated, given its iterative transmission of substantial representations and gradients, SplitNN often outperforms other methods across a majority of datasets. Comparatively, the performance of FedTree and GAL is dataset-dependent. FedTree is well-suited to high-dimensional, smaller datasets like gisette, but struggles with larger datasets like epsilon and covtype. GAL, on the other hand, performs admirably with binary classification and regression tasks, though its performance drops significantly as the number of classes increases, as observed on the covtype and letter dataset.

The compression of SplitNN-based methods, particularly when employed on imbalanced partitioned datasets, can significantly impact accuracy. While C-VFL’s model structure is akin to SplitNN, the incorporation of compression results in C-VFL having the lowest accuracy among all the tested baselines. This is particularly pronounced in cases of imbalanced importance distribution, i.e., smaller α . For example, when $\alpha = 0.1$, C-VFL’s performance on the letter and epsilon datasets is barely superior to random guessing. This highlights a pressing need for further exploration and development of compression methods suited for biased partition scenarios.

Table 2: Accuracy/RMSE of VFL algorithms on different datasets varying imbalance and correlation

Dataset	Method	Performance of importance-based split				Performance of correlation-based split			
		$\alpha = 0.1$	$\alpha = 1$	$\alpha = 10$	$\alpha = 100$	$\beta = 0$	$\beta = 0.3$	$\beta = 0.6$	$\beta = 1$
covtype	SplitNN	91.2±0.4%	92.1±0.2%	92.1±0.3%	92.1±0.1%	91.7±0.3%	91.8±0.2%	92.1±0.1%	92.3±0.2%
	GAL	66.1±2.9%	60.2±1.1%	62.1±4.1%	61.5±3.9%	63.9±1.2%	62.5±1.7%	61.8±1.6%	61.8±1.8%
	FedTree	77.9±0.1%	77.8±0.2%	77.8±0.1%	77.8±0.1%	77.9±0.1%	77.9±0.2%	77.8±0.1%	77.8±0.1%
	C-VFL	46.9±4.1%	14.8±19.0%	26.9±25.3%	38.3±18.6%	53.6±6.8%	50.1±1.8%	49.0±9.0%	49.5±1.0%
msd	SplitNN	10.1±0.0%	10.2±0.0%	10.1±0.0%	10.1±0.0%	10.2±0.0%	10.1±0.0%	10.2±0.0%	10.1±0.0%
	GAL	12.2±0.0%	12.2±0.0%	12.2±0.0%	12.2±0.0%	12.2±0.0%	12.2±0.0%	12.2±0.0%	12.2±0.0%
	FedTree	10.4±0.0%	10.4±0.0%	10.4±0.0%	10.4±0.0%	10.4±0.0%	10.4±0.0%	10.4±0.0%	10.4±0.0%
	C-VFL	12.7±0.0%	12.7±0.0%	12.7±0.0%	12.7±0.0%	12.3±0.0%	12.2±0.0%	12.1±0.1%	12.3±0.0%
gisette	SplitNN	96.8±0.4%	96.8±0.3%	96.9±0.3%	96.9±0.2%	97.1±0.2%	97.2±0.4%	97.0±0.1%	96.8±0.4%
	GAL	94.4±1.7%	95.7±0.6%	96.2±0.6%	96.1±0.6%	96.5±0.3%	96.9±0.2%	96.6±0.3%	96.9±0.1%
	FedTree	97.0±0.3%	97.1±0.5%	97.1±0.5%	97.1±0.3%	97.0±0.4%	96.9±0.3%	97.1±0.2%	97.0±0.3%
	C-VFL	91.0±11.5%	97.8±3.4%	90.1±11.8%	94.0±4.0%	90.1±8.8%	97.6±4.1%	97.6±4.1%	93.6±5.2%
realsim	SplitNN	97.1±0.0%	97.0±0.0%	97.0±0.1%	97.1±0.1%	97.0±0.0%	97.0±0.2%	97.0±0.1%	97.0±0.1%
	GAL	92.4±0.7%	93.5±2.2%	96.1±0.4%	96.4±0.1%	96.5±0.1%	96.5±0.0%	96.5±0.0%	96.5±0.1%
	FedTree	85.1±0.2%	85.2±0.2%	85.1±0.1%	85.1±0.2%	85.2±0.2%	85.2±0.2%	85.1±0.2%	85.2±0.1%
	C-VFL	89.6±17.4%	88.6±16.7%	89.5±17.4%	87.8±16.1%	89.3±17.2%	89.3±17.2%	87.8±16.2%	89.2±17.0%
epsilon	SplitNN	86.3±0.1%	86.2±0.1%	86.3±0.0%	86.2±0.0%	85.9±0.1%	85.9±0.0%	86.0±0.1%	86.2±0.1%
	GAL	88.2±0.6%	85.9±1.5%	85.7±0.4%	86.3±0.2%	86.1±0.0%	86.1±0.4%	86.3±0.3%	86.4±0.2%
	FedTree	77.2±0.1%	77.3±0.1%	77.2±0.0%	77.2±0.1%	77.3±0.1%	77.3±0.0%	77.3±0.0%	77.3±0.1%
	C-VFL	50.1±0.0%	53.5±4.9%	67.7±20.0%	61.6±16.4%	70.5±28.9%	65.8±22.3%	53.4±4.7%	60.8±15.1%
letter	SplitNN	95.5±0.3%	96.0±0.3%	96.1±0.2%	96.0±0.3%	96.3±0.2%	96.0±0.3%	96.2±0.3%	96.1±0.2%
	GAL	57.9±4.1%	51.4±3.1%	52.0±4.3%	49.1±2.6%	49.1±2.2%	50.0±3.0%	48.3±4.4%	48.8±2.0%
	FedTree	91.7±0.3%	91.9±0.4%	92.0±0.3%	92.0±0.3%	92.0±0.2%	92.0±0.2%	91.9±0.4%	91.9±0.3%
	C-VFL	5.0±1.0%	12.6±8.3%	37.1±47.1%	43.8±4.5%	34.8±45.0%	8.1±1.9%	3.6±0.7%	33.6±39.8%
radar	SplitNN	99.7±0.0%	99.8±0.0%	99.8±0.0%	99.8±0.0%	99.8±0.0%	99.8±0.0%	99.8±0.0%	99.8±0.0%
	GAL	90.0±3.6%	95.9±2.5%	97.5±0.4%	97.9±0.1%	96.7±0.1%	96.9±0.2%	97.6±0.4%	97.7±0.3%
	FedTree	99.3±0.0%	99.3±0.0%	99.3±0.0%	99.3±0.0%	99.3±0.0%	99.3±0.0%	99.3±0.0%	99.3±0.0%
	C-VFL	59.9±47.8%	53.4±38.5%	43.1±23.9%	37.3±15.7%	30.6±6.3%	53.8±39.0%	60.8±49.0%	54.4±39.9%

6.3 Communication Efficiency

In this subsection, we evaluate VFL algorithms’ communication efficiency by analyzing their total communication size within 50 fixed epochs, as shown in Figure 3. Additional communication details, such as the maximum incoming and outgoing communication, are provided in Appendix G.1. Given that FedTree, Pivot, and SecureBoost incur comparable communication costs when excluding encryption overhead, we will utilize FedTree as a representative for the other two for simplicity. Upon examining the figure, two main observations can be drawn.

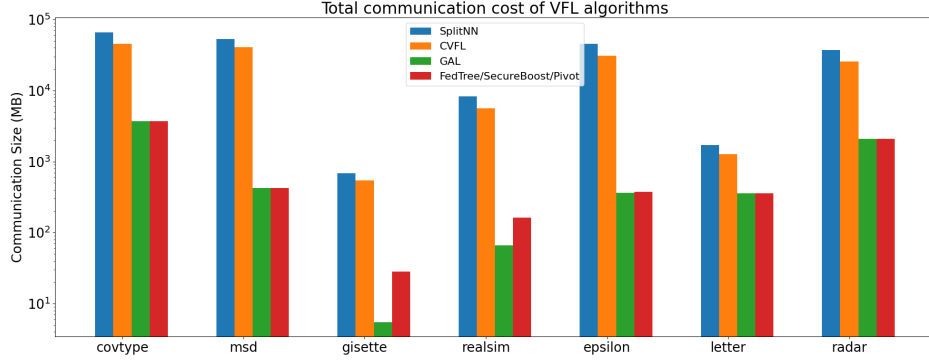


Figure 3: The total communication size of VFL algorithms (50 global iterations)

Gradient-boosting algorithms, including GAL and FedTree, generally exhibit smaller communication sizes compared to neural-network-based algorithms like SplitNN and C-VFL, with the exception of the letter dataset with 26 classes. C-VFL’s compression techniques, though limiting its communication size, cannot match the efficiency of GAL and FedTree, even with a significant accuracy trade-off. The higher communication cost in neural networks is due to frequent transmission of gradients and representations, a factor that boosts SplitNN’s optimal accuracy.

Additionally, **the efficiency of FedTree and GAL is contingent on the global dataset’s size**. The primary distinction between FedTree and GAL lies in the type of information received on the primary party side. GAL collates prediction results from all secondary parties, with the size being proportional to the number of instances. Conversely, FedTree gathers the histogram from all secondary parties, with the size being proportional to the number of features. Consequently, GAL incurs lower communication costs than FedTree on high-dimensional datasets, such as gisette and realsim, while maintaining comparable communication costs on other datasets.

7 Conclusion

In this study, we introduce VertiBench, a versatile benchmarking framework for Vertical Federated Learning (VFL). VertiBench facilitates the synthetic generation of diverse VFL datasets from a single global set, thereby enabling a comprehensive performance assessment of VFL algorithms across a wide spectrum of application domains. Our empirical results reveal potential significant variations in algorithm performance under different data partition scenarios, underscoring the importance of our benchmark. Additionally, we contribute a new real-world VFL dataset, addressing a deficit in image-image VFL datasets. This study highlights the necessity of examining VFL algorithms under diverse data distribution conditions, providing a crucial trajectory for future research.

References

- [1] Tom Brown, Benjamin Mann, Nick Ryder, Melanie Subbiah, Jared D Kaplan, Prafulla Dhariwal, Arvind Neelakantan, Pranav Shyam, Girish Sastry, Amanda Askell, et al. Language models are few-shot learners. *Advances in neural information processing systems*, 33:1877–1901, 2020.
- [2] Paul Voigt and Axel Von dem Bussche. The eu general data protection regulation (gdpr). *A Practical Guide, 1st Ed., Cham: Springer International Publishing*, 10(3152676):10–5555, 2017.
- [3] Jakub Konečný, H Brendan McMahan, Felix X Yu, Peter Richtárik, Ananda Theertha Suresh, and Dave Bacon. Federated learning: Strategies for improving communication efficiency. *arXiv preprint arXiv:1610.05492*, 2016.
- [4] Qinbin Li, Zeyi Wen, Zhaomin Wu, Sixu Hu, Naibo Wang, Yuan Li, Xu Liu, and Bingsheng He. A survey on federated learning systems: vision, hype and reality for data privacy and protection. *IEEE Transactions on Knowledge and Data Engineering*, 2021.

- [5] Enmao Diao, Jie Ding, and Vahid Tarokh. Gal: Gradient assisted learning for decentralized multi-organization collaborations. In S. Koyejo, S. Mohamed, A. Agarwal, D. Belgrave, K. Cho, and A. Oh, editors, *Advances in Neural Information Processing Systems*, volume 35, pages 11854–11868. Curran Associates, Inc., 2022. URL https://proceedings.neurips.cc/paper_files/paper/2022/file/4d6938f94ab47d32128c239a4bfedae0-Paper-Conference.pdf.
- [6] Xun Xian, Xinran Wang, Jie Ding, and Reza Ghanadan. Assisted learning: A framework for multi-organization learning. In H. Larochelle, M. Ranzato, R. Hadsell, M.F. Balcan, and H. Lin, editors, *Advances in Neural Information Processing Systems*, volume 33, pages 14580–14591. Curran Associates, Inc., 2020. URL https://proceedings.neurips.cc/paper_files/paper/2020/file/a7b23e6eefbe6cf04b8e62a6f0915550-Paper.pdf.
- [7] Praneeth Vepakomma, Otakrist Gupta, Tristan Swedish, and Ramesh Raskar. Split learning for health: Distributed deep learning without sharing raw patient data. *arXiv preprint arXiv:1812.00564*, 2018.
- [8] Jiayi Chen and Aidong Zhang. Fedmsplit: Correlation-adaptive federated multi-task learning across multimodal split networks. In *Proceedings of the 28th ACM SIGKDD Conference on Knowledge Discovery and Data Mining*, KDD ’22, page 87–96, New York, NY, USA, 2022. Association for Computing Machinery. ISBN 9781450393850. doi: 10.1145/3534678.3539384. URL <https://doi-org.libproxy1.nus.edu.sg/10.1145/3534678.3539384>.
- [9] Hangyu Zhu, Jinjin Xu, Shiqing Liu, and Yaochu Jin. Federated learning on non-iid data: A survey. *Neurocomputing*, 465:371–390, 2021.
- [10] Liu Yang, Di Chai, Junxue Zhang, Yilun Jin, Leye Wang, Hao Liu, Han Tian, Qian Xu, and Kai Chen. A survey on vertical federated learning: From a layered perspective. *arXiv preprint arXiv:2304.01829*, 2023.
- [11] Fan Lai, Yinwei Dai, Sanjay Singapuram, Jiachen Liu, Xiangfeng Zhu, Harsha Madhyastha, and Mosharaf Chowdhury. Fedscale: Benchmarking model and system performance of federated learning at scale. In *International Conference on Machine Learning*, pages 11814–11827. PMLR, 2022.
- [12] Geun Hyeong Lee and Soo-Yong Shin. Federated learning on clinical benchmark data: performance assessment. *Journal of medical Internet research*, 22(10):e20891, 2020.
- [13] Di Chai, Leye Wang, Kai Chen, and Qiang Yang. Fedeval: A benchmark system with a comprehensive evaluation model for federated learning. *arXiv preprint arXiv:2011.09655*, 2020.
- [14] Qinbin Li, Yiqun Diao, Quan Chen, and Bingsheng He. Federated learning on non-iid data silos: An experimental study. In *2022 IEEE 38th International Conference on Data Engineering (ICDE)*, pages 965–978. IEEE, 2022.
- [15] Sixu Hu, Yuan Li, Xu Liu, Qinbin Li, Zhaomin Wu, and Bingsheng He. The oarf benchmark suite: Characterization and implications for federated learning systems. *ACM Transactions on Intelligent Systems and Technology (TIST)*, 13(4):1–32, 2022.
- [16] Tat-Seng Chua, Jinhui Tang, Richang Hong, Haojie Li, Zhiping Luo, and Yan-Tao Zheng. Nus-wide: A real-world web image database from national university of singapore. In *Proc. of ACM Conf. on Image and Video Retrieval (CIVR’09)*, Santorini, Greece., July 8-10, 2009.
- [17] Marco F Duarte and Yu Hen Hu. Vehicle classification in distributed sensor networks. *Journal of Parallel and Distributed Computing*, 64(7):826–838, 2004.
- [18] Chaoyang He, Songze Li, Jinhyun So, Xiao Zeng, Mi Zhang, Hongyi Wang, Xiaoyang Wang, Praneeth Vepakomma, Abhishek Singh, Hang Qiu, et al. Fedml: A research library and benchmark for federated machine learning. *arXiv preprint arXiv:2007.13518*, 2020.
- [19] Sebastian Caldas, Sai Meher Karthik Duddu, Peter Wu, Tian Li, Jakub Konečný, H Brendan McMahan, Virginia Smith, and Ameet Talwalkar. Leaf: A benchmark for federated settings. *arXiv preprint arXiv:1812.01097*, 2018.

- [20] Yaochen Hu, Di Niu, Jianming Yang, and Shengping Zhou. Fdml: A collaborative machine learning framework for distributed features. In *Proceedings of the 25th ACM SIGKDD International Conference on Knowledge Discovery & Data Mining*, KDD '19, page 2232–2240, New York, NY, USA, 2019. Association for Computing Machinery. ISBN 9781450362016. doi: 10.1145/3292500.3330765. URL <https://doi-org.libproxy1.nus.edu.sg/10.1145/3292500.3330765>.
- [21] Timothy J Castiglia, Anirban Das, Shiqiang Wang, and Stacy Patterson. Compressed-VFL: Communication-efficient learning with vertically partitioned data. In Kamalika Chaudhuri, Stefanie Jegelka, Le Song, Csaba Szepesvari, Gang Niu, and Sivan Sabato, editors, *Proceedings of the 39th International Conference on Machine Learning*, volume 162 of *Proceedings of Machine Learning Research*, pages 2738–2766. PMLR, 17–23 Jul 2022. URL <https://proceedings.mlr.press/v162/castiglia22a.html>.
- [22] Kewei Cheng, Tao Fan, Yilun Jin, Yang Liu, Tianjian Chen, Dimitrios Papadopoulos, and Qiang Yang. Secureboost: A lossless federated learning framework. *IEEE Intelligent Systems*, 36(6): 87–98, 2021.
- [23] Shay Cohen, Eytan Ruppín, and Gideon Dror. Feature selection based on the shapley value. *other words*, 1(98Eqr):155, 2005.
- [24] I Elizabeth Kumar, Suresh Venkatasubramanian, Carlos Scheidegger, and Sorelle Friedler. Problems with shapley-value-based explanations as feature importance measures. In *International Conference on Machine Learning*, pages 5491–5500. PMLR, 2020.
- [25] Sisi Ma and Roshan Tourani. Predictive and causal implications of using shapley value for model interpretation. In *Proceedings of the 2020 KDD workshop on causal discovery*, pages 23–38. PMLR, 2020.
- [26] Guan Wang, Charlie Xiaoqian Dang, and Ziyue Zhou. Measure contribution of participants in federated learning. In *2019 IEEE international conference on big data (Big Data)*, pages 2597–2604. IEEE, 2019.
- [27] Guan Wang. Interpret federated learning with shapley values. *arXiv preprint arXiv:1905.04519*, 2019.
- [28] Xiao Han, Leye Wang, and Junjie Wu. Data valuation for vertical federated learning: An information-theoretic approach. *arXiv preprint arXiv:2112.08364*, 2021.
- [29] Qinbin Li, Zhaomin Wu, Yanzheng Cai, Yuxuan Han, Ching Man Yung, Tianyuan Fu, and Bingsheng He. Fedtree: A federated learning system for trees. In *Proceedings of Machine Learning and Systems*, 2023.
- [30] Leann Myers and Maria J Sirois. Spearman correlation coefficients, differences between. *Encyclopedia of statistical sciences*, 12, 2004.
- [31] Joost CF De Winter, Samuel D Gosling, and Jeff Potter. Comparing the pearson and spearman correlation coefficients across distributions and sample sizes: A tutorial using simulations and empirical data. *Psychological methods*, 21(3):273, 2016.
- [32] Mukund Sundararajan, Kedar Dhamdhere, and Ashish Agarwal. The shapley taylor interaction index. In *International conference on machine learning*, pages 9259–9268. PMLR, 2020.
- [33] Jianji Wang and Nanning Zheng. Measures of correlation for multiple variables. *arXiv preprint arXiv:1401.4827*, 2014.
- [34] Benjamin M Taylor. A multi-way correlation coefficient. *arXiv preprint arXiv:2003.02561*, 2020.
- [35] Xiao Jin, Pin-Yu Chen, Chia-Yi Hsu, Chia-Mu Yu, and Tianyi Chen. Cafe: Catastrophic data leakage in vertical federated learning. In M. Ranzato, A. Beygelzimer, Y. Dauphin, P.S. Liang, and J. Wortman Vaughan, editors, *Advances in Neural Information Processing Systems*, volume 34, pages 994–1006. Curran Associates, Inc., 2021. URL https://proceedings.neurips.cc/paper_files/paper/2021/file/08040837089cdf46631a10aca5258e16-Paper.pdf.

- [36] Tao Qi, Fangzhao Wu, Chuhan Wu, Lingjuan Lyu, Tong Xu, Hao Liao, Zhongliang Yang, Yongfeng Huang, and Xing Xie. Fairvfl: A fair vertical federated learning framework with contrastive adversarial learning. In S. Koyejo, S. Mohamed, A. Agarwal, D. Belgrave, K. Cho, and A. Oh, editors, *Advances in Neural Information Processing Systems*, volume 35, pages 7852–7865. Curran Associates, Inc., 2022. URL https://proceedings.neurips.cc/paper_files/paper/2022/file/333a7697dbb67f09249337f81c27d749-Paper-Conference.pdf.
- [37] Jiawei Jiang, Lukas Burkhalter, Fangcheng Fu, Bolin Ding, Bo Du, Anwar Hithnawi, Bo Li, and Ce Zhang. Vf-ps: How to select important participants in vertical federated learning, efficiently and securely? In *Advances in Neural Information Processing Systems*, 2022.
- [38] Qingsong Zhang, Bin Gu, Cheng Deng, and Heng Huang. Secure bilevel asynchronous vertical federated learning with backward updating. In *Proceedings of the AAAI Conference on Artificial Intelligence*, volume 35, pages 10896–10904, 2021.
- [39] Qingsong Zhang, Bin Gu, Cheng Deng, Songxiang Gu, Liefeng Bo, Jian Pei, and Heng Huang. Asysqn: Faster vertical federated learning algorithms with better computation resource utilization. In *Proceedings of the 27th ACM SIGKDD Conference on Knowledge Discovery & Data Mining, KDD '21*, page 3917–3927, New York, NY, USA, 2021. Association for Computing Machinery. ISBN 9781450383325. doi: 10.1145/3447548.3467169. URL <https://doi-org.libproxy1.nus.edu.sg/10.1145/3447548.3467169>.
- [40] Fangcheng Fu, Xupeng Miao, Jiawei Jiang, Huanran Xue, and Bin Cui. Towards communication-efficient vertical federated learning training via cache-enabled local updates. *Proc. VLDB Endow.*, 15(10):2111–2120, jun 2022. ISSN 2150-8097. doi: 10.14778/3547305.3547316. URL <https://doi-org.libproxy1.nus.edu.sg/10.14778/3547305.3547316>.
- [41] Qi Chang, Hui Qu, Yikai Zhang, Mert Sabuncu, Chao Chen, Tong Zhang, and Dimitris N. Metaxas. Synthetic learning: Learn from distributed asynchronized discriminator gan without sharing medical image data. In *Proceedings of the IEEE/CVF Conference on Computer Vision and Pattern Recognition (CVPR)*, June 2020.
- [42] Zitao Li, Bolin Ding, Ce Zhang, Ninghui Li, and Jingren Zhou. Federated matrix factorization with privacy guarantee. *Proc. VLDB Endow.*, 15(4):900–913, dec 2021. ISSN 2150-8097. doi: 10.14778/3503585.3503598. URL <https://doi-org.libproxy1.nus.edu.sg/10.14778/3503585.3503598>.
- [43] Lingxiao Huang, Zhize Li, Jialin Sun, and Haoyu Zhao. Coresets for vertical federated learning: Regularized linear regression and k-means clustering. In S. Koyejo, S. Mohamed, A. Agarwal, D. Belgrave, K. Cho, and A. Oh, editors, *Advances in Neural Information Processing Systems*, volume 35, pages 29566–29581. Curran Associates, Inc., 2022. URL https://proceedings.neurips.cc/paper_files/paper/2022/file/be7b70477c8fca697f14b1dbb1c086d1-Paper-Conference.pdf.
- [44] Zhaomin Wu, Qinbin Li, and Bingsheng He. A coupled design of exploiting record similarity for practical vertical federated learning. In S. Koyejo, S. Mohamed, A. Agarwal, D. Belgrave, K. Cho, and A. Oh, editors, *Advances in Neural Information Processing Systems*, volume 35, pages 21087–21100. Curran Associates, Inc., 2022. URL https://proceedings.neurips.cc/paper_files/paper/2022/file/84b744165a0597360caad96b06e69313-Paper-Conference.pdf.
- [45] Richard Nock, Stephen Hardy, Wilko Henecka, Hamish Ivey-Law, Jakub Nabaglo, Giorgio Patrini, Guillaume Smith, and Brian Thorne. The impact of record linkage on learning from feature partitioned data. In Marina Meila and Tong Zhang, editors, *Proceedings of the 38th International Conference on Machine Learning*, volume 139 of *Proceedings of Machine Learning Research*, pages 8216–8226. PMLR, 18–24 Jul 2021. URL <https://proceedings.mlr.press/v139/nock21a.html>.
- [46] Xun Xian, Xinran Wang, Jie Ding, and Reza Ghanadan. Assisted learning: A framework for multi-organization learning. https://proceedings.neurips.cc/paper_files/paper/2020/file/a7b23e6eefbe6cf04b8e62a6f0915550-Supplemental.zip, 2020.

- [47] Enmao Diao, Jie Ding, and Vahid Tarokh. Gal: Gradient assisted learning for decentralized multi-organization collaborations. <https://github.com/dem123456789/GAL-Gradient-Assisted-Learning-for-Decentralized-Multi-Organization-Collaborations>, 2022.
- [48] Zhaomin Wu. A coupled design of exploiting record similarity for practical vertical federated learning, 2022.
- [49] Timothy J Castiglia, Anirban Das, Shiqiang Wang, and Stacy Patterson. Compressed-VFL: Communication-efficient learning with vertically partitioned data. <https://media.icml.cc/Conferences/ICML2022/supplementary/castiglia22a-sup.zip>, 2022.
- [50] Fangcheng Fu, Huanran Xue, Yong Cheng, Yangyu Tao, and Bin Cui. Blindfl: Vertical federated machine learning without peeking into your data. In *Proceedings of the 2022 International Conference on Management of Data*, SIGMOD '22, page 1316–1330, New York, NY, USA, 2022. Association for Computing Machinery. ISBN 9781450392495. doi: 10.1145/3514221.3526127. URL <https://doi-org.libproxy1.nus.edu.sg/10.1145/3514221.3526127>.
- [51] Kewei Cheng, Tao Fan, Yilun Jin, Yang Liu, Tianjian Chen, Dimitrios Papadopoulos, and Qiang Yang. Secureboost: A lossless federated learning framework. https://github.com/FederatedAI/FATE/tree/master/python/federatedml/ensemble/secureboost/hetero_secureboost, 2021.
- [52] Yuncheng Wu, Shaofeng Cai, Xiaokui Xiao, Gang Chen, and Beng Chin Ooi. Privacy preserving vertical federated learning for tree-based models. *Proc. VLDB Endow.*, 13(12):2090–2103, jul 2020. ISSN 2150-8097. doi: 10.14778/3407790.3407811. URL <https://doi-org.libproxy1.nus.edu.sg/10.14778/3407790.3407811>.
- [53] Yuncheng Wu, Shaofeng Cai, Xiaokui Xiao, Gang Chen, and Beng Chin Ooi. Privacy preserving vertical federated learning for tree-based models. <https://github.com/nusdbsystem/pivot>, 2020.
- [54] Qinbin Li, Zhaomin Wu, Yanzheng Cai, Yuxuan Han, Ching Man Yung, Tianyuan Fu, and Bingsheng He. Fedtree: A fast, effective, and secure tree-based federated learning system. https://github.com/Xtra-Computing/FedTree/blob/main/FedTree_draft_paper.pdf, 2022.
- [55] Fangcheng Fu, Yingxia Shao, Lele Yu, Jiawei Jiang, Huanran Xue, Yangyu Tao, and Bin Cui. Vf2boost: Very fast vertical federated gradient boosting for cross-enterprise learning. In *Proceedings of the 2021 International Conference on Management of Data*, SIGMOD '21, page 563–576, New York, NY, USA, 2021. Association for Computing Machinery. ISBN 9781450383431. doi: 10.1145/3448016.3457241. URL <https://doi-org.libproxy1.nus.edu.sg/10.1145/3448016.3457241>.
- [56] Tianqi Chen and Carlos Guestrin. Xgboost: A scalable tree boosting system. In *Proceedings of the 22nd acm sigkdd international conference on knowledge discovery and data mining*, pages 785–794, 2016.
- [57] Stephen Hardy, Wilko Henecka, Hamish Ivey-Law, Richard Nock, Giorgio Patrini, Guillaume Smith, and Brian Thorne. Private federated learning on vertically partitioned data via entity resolution and additively homomorphic encryption. *arXiv preprint arXiv:1711.10677*, 2017.
- [58] Bin Gu, Zhiyuan Dang, Xiang Li, and Heng Huang. Federated doubly stochastic kernel learning for vertically partitioned data. In *Proceedings of the 26th ACM SIGKDD International Conference on Knowledge Discovery & Data Mining*, KDD '20, page 2483–2493, New York, NY, USA, 2020. Association for Computing Machinery. ISBN 9781450379984. doi: 10.1145/3394486.3403298. URL <https://doi-org.libproxy1.nus.edu.sg/10.1145/3394486.3403298>.
- [59] Jerrold H Zar. Spearman rank correlation. *Encyclopedia of biostatistics*, 7, 2005.
- [60] José Fernando Gonçalves and Mauricio GC Resende. Biased random-key genetic algorithms for combinatorial optimization. *Journal of Heuristics*, 17(5):487–525, 2011.

- [61] Kirk Baker. Singular value decomposition tutorial. *The Ohio State University*, 24, 2005.
- [62] Per Christian Hansen. Truncated singular value decomposition solutions to discrete ill-posed problems with ill-determined numerical rank. *SIAM Journal on Scientific and Statistical Computing*, 11(3):503–518, 1990.
- [63] Julien Cornebise, Ivan Oršolić, and Freddie Kalaitzis. Open high-resolution satellite imagery: The worldstrat dataset –with application to super-resolution. In S. Koyejo, S. Mohamed, A. Agarwal, D. Belgrave, K. Cho, and A. Oh, editors, *Advances in Neural Information Processing Systems*, volume 35, pages 25979–25991. Curran Associates, Inc., 2022. URL https://proceedings.neurips.cc/paper_files/paper/2022/file/a6fe99561d9eb9c90b322afe664587fd-Paper-Datasets_and_Benchmarks.pdf.
- [64] Coverttype, 1998. URL <https://www.csie.ntu.edu.tw/~cjlin/libsvmtools/datasets/multiclass/covtype.bz2>.
- [65] Yearpredictionmsd, 2011. URL <https://www.csie.ntu.edu.tw/~cjlin/libsvmtools/datasets/regression/YearPredictionMSD.bz2>.
- [66] Gisette, 2008. URL https://www.csie.ntu.edu.tw/~cjlin/libsvmtools/datasets/binary/gisette_scale.bz2.
- [67] Real vs. simulated, 2015. URL <https://www.csie.ntu.edu.tw/~cjlin/libsvmtools/datasets/binary/real-sim.bz2>.
- [68] Epsilon, 2008. URL https://www.csie.ntu.edu.tw/~cjlin/libsvmtools/datasets/binary/epsilon_normalized.bz2.
- [69] Letter, 1991. URL <https://www.csie.ntu.edu.tw/~cjlin/libsvmtools/datasets/multiclass/letter.scale>.
- [70] Iman Khosravi. UCI machine learning repository, 06 2020. URL <https://archive.ics.uci.edu/ml/machine-learning-databases/00525/data.zip>.
- [71] Attribution 4.0 international, 2023. URL <https://creativecommons.org/licenses/by/4.0/legalcode>.
- [72] Attribution-noncommercial 4.0 international (cc by-nc 4.0), 2023. URL <https://creativecommons.org/licenses/by-nc/4.0/>.
- [73] Anonymized, 2023. URL <https://drive.google.com/drive/folders/1Ti73Doy7xW0BRv2D8FHZFqS1zZWfd2gj>.
- [74] The 3-clause bsd license, 2023. URL <https://opensource.org/license/bsd-3-clause/>.
- [75] Attribution-noncommercial-sharealike 2.0 generic (cc by-nc-sa 2.0), 2023. URL <https://creativecommons.org/licenses/by-nc-sa/2.0/>.
- [76] The mit license, 2023. URL <https://opensource.org/license/mit/>.
- [77] Apache license, version 2.0, 2023. URL <https://www.apache.org/licenses/LICENSE-2.0>.
- [78] Attribution-noncommercial-noderivatives 4.0 international (cc by-nc-nd 4.0), 2023. URL <https://creativecommons.org/licenses/by-nc-nd/4.0/>.

Appendix

Table of Contents

A Proof	15
B Details of VFL Algorithms	17
B.1 Ensemble-based VFL Algorithms	17
B.2 Split-NN-based VFL Algorithms	17
B.3 Split-GBDT-based VFL Algorithms	18
C Split Method Details	19
D Empirical Validation of Split Methods	20
D.1 Correlation Evaluation Metric	20
D.2 Correlation-based Feature-split Algorithm	20
D.3 Time Efficiency of Split Methods.	21
E Real Dataset Construction	21
F Experimental Details	22
G Additional Experiments	23
G.1 Communication Cost Details	23
G.2 Scalability	23
G.3 Training Time	25
G.4 Performance on Satellite dataset	25
H Discussion	25
H.1 Limitations	26
H.2 Social Impacts	26

A Proof

Proposition 1. *The probability mass function can be written as*

$$\log \mathcal{P}(y|X_K, \dots, X_1) = \sum_{i=1}^K \log \frac{\mathcal{P}(y|X_k, \dots, X_1)}{\mathcal{P}(y|X_{k-1}, \dots, X_1)} + \log \mathcal{P}(y) \quad (4)$$

Proof. According to the definition of conditional probability, this marginal distribution can be written as

$$\begin{aligned} & \mathcal{P}(y|X_K, \dots, X_1) \\ &= \frac{\mathcal{P}(y, X_K, \dots, X_1)}{\mathcal{P}(X_K, \dots, X_1)} \\ &= \frac{\mathcal{P}(y)\mathcal{P}(X_1|y) \prod_{k=2}^K \mathcal{P}(X_k|y, X_{k-1}, \dots, X_1)}{\mathcal{P}(X_1) \prod_{k=2}^K \mathcal{P}(X_k|X_{k-1}, \dots, X_1)} \\ &= \mathcal{P}(y) \frac{\mathcal{P}(X_1|y)}{\mathcal{P}(X_1)} \prod_{k=2}^K \frac{\mathcal{P}(X_k|y, X_{k-1}, \dots, X_1)}{\mathcal{P}(X_k|X_{k-1}, \dots, X_1)} \end{aligned} \quad (5)$$

Denoting

$$c_k = \log \frac{\mathcal{P}(X_k|y, X_{k-1}, \dots, X_1)}{\mathcal{P}(X_k|X_{k-1}, \dots, X_1)}, \quad c_1 = \log \frac{\mathcal{P}(X_1|y)}{\mathcal{P}(X_1)} \quad (6)$$

Adding logarithm on both sides, we have

$$\log \mathcal{P}(y|X_K, \dots, X_1) = \sum_{i=1}^K \log c_i + \log \mathcal{P}(y) \quad (7)$$

Furthermore, we have

$$\begin{aligned} c_k &= \frac{\mathcal{P}(X_k|y, X_{k-1}, \dots, X_1)}{\mathcal{P}(X_k|X_{k-1}, \dots, X_1)} \\ &= \frac{\mathcal{P}(X_k, y|X_{k-1}, \dots, X_1)}{\mathcal{P}(X_k|X_{k-1}, \dots, X_1) \mathcal{P}(y|X_{k-1}, \dots, X_1)} \\ &= \frac{\mathcal{P}(y|X_k, \dots, X_1)}{\mathcal{P}(y|X_{k-1}, \dots, X_1)} \end{aligned} \quad (8)$$

Combining (6) and (8), we have

$$\log \mathcal{P}(y|X_K, \dots, X_1) = \sum_{i=1}^K \log \frac{\mathcal{P}(y|X_i, \dots, X_1)}{\mathcal{P}(y|X_{i-1}, \dots, X_1)} + \log \mathcal{P}(y) \quad (9)$$

□

Theorem 1. Consider a feature index set $\mathcal{A} = \{1, 2, \dots, m\}$ and a characteristic function $v : 2^{\mathcal{A}} \rightarrow \mathbb{R}$ such that $v(\emptyset) = 0$. Let $\phi_j(v)$ denote the importance of the j -th feature on v such that $\sum_{j=1}^m \phi(j) = v(\mathcal{A})$. Assume that the indices in \mathcal{A} are randomly distributed to K parties with probabilities r_1, \dots, r_K where $\sum_{i=1}^K r_i = 1$. Given budgets $b_i = r_i v(\mathcal{A})$, let Z_i be the sum of feature importance for party i . Then, we have $\forall i \in [1, K], \mathbf{E}[Z_i] = b_i$ and $\mathbf{E}[Z_i] \propto r_i$.

Proof. For each feature j assigned to party i with probability r_i , we define the feature importance Y_{ij} as:

$$Y_{ij} = \begin{cases} \phi_j(v), & \text{w.p. } r_i \\ 0, & \text{w.p. } 1 - r_i \end{cases} \quad (10)$$

By leveraging the property of linearity of expectation, we find that:

$$\mathbf{E}[Z_i] = \sum_{j=1}^m \mathbf{E}[Y_{ij}] = \sum_{j=1}^m \phi_j(v) r_i = r_i \sum_{j=1}^m \phi(j) \quad (11)$$

Given that $\sum_{j=1}^m \phi(j) = v(\mathcal{A})$, we derive:

$$\mathbf{E}[Z_i] = b_i \quad (12)$$

Moreover, since $v(\mathcal{A})$ is a constant, it follows that:

$$\mathbf{E}[Z_i] \propto r_i \quad (13)$$

□

Proposition 2. Given a Dirichlet distribution $\text{Dir}(\alpha_1, \dots, \alpha_K)$ with mean variance σ , symmetric Dirichlet distribution $\text{Dir}(\bar{\alpha})$ that has the same mean variance σ if $\bar{\alpha} = \frac{K-1-K^2\sigma}{K^3\sigma}$.

Proof. Suppose we have variables X_1, \dots, X_K following the Dirichlet distribution, denoted as $\text{Dir}(\bar{\alpha}, \dots, \bar{\alpha})$. Leveraging the inherent properties of the Dirichlet distribution, we can formulate the variance $\text{Var}(X_i)$ for all $i \in [1, K]$ as

$$\text{Var}(X_i) = \frac{K-1}{K^2(K\bar{\alpha}+1)} \quad (14)$$

The mean variance, denoted as σ , can subsequently be articulated in terms of the expected variance, $\mathbb{E}[\text{Var}(X_i)]$, as

$$\mathbb{E}[\text{Var}(X_i)] = \frac{K-1}{K^2(K\bar{\alpha}+1)} = \sigma \quad (15)$$

Recognizing that for a Dirichlet distribution $\sigma > 0$ holds, we can transform the above equation to express $\bar{\alpha}$ in terms of σ :

$$\bar{\alpha} = \frac{K-1-K^2\sigma}{K^3\sigma} \quad (16)$$

□

B Details of VFL Algorithms

In this section, we provide a detailed comparison of the existing VFL algorithms as an extension of Table 1.

B.1 Ensemble-based VFL Algorithms

In the ensemble-based VFL algorithms detailed in Algorithm 2, each iteration t commences with the primary party P_1 calculating the residual of the prior global model $F^{t-1}(\cdot)$ (line 3). This is followed by the communication of residuals \mathbf{r}_1^t to the secondary parties (P_2, \dots, P_K). In the ensuing step (line 5), each secondary party trains a local model $f(\theta_i^t; \cdot)$ on its local data \mathbf{X}_i to predict the residuals, subsequently sending the model parameters θ_i^t back to P_1 . P_1 then aggregates these local models and updates the global model $F^t(\cdot)$ (line 6). This process iterates until a convergence criterion is achieved.

Specifics of residual sharing and model aggregation depend on algorithm design. In AL, residuals are shared among parties, and models are aggregated through summation. Conversely, in GAL, pseudo residuals (i.e., gradients) are shared, and models are aggregated through a weighted summation. Furthermore, the aggregation weight in GAL can be updated during the training process.

Algorithm 2: Outline of ensemble-based VFL algorithms

Input : Number of iterations T ; number of parties K ; data and labels of primary party \mathbf{X}_1, \mathbf{y} , learning rate η^t ; data of secondary parties $\mathbf{X}_2, \dots, \mathbf{X}_K$
Output : Models on K parties $f(\theta_1; \cdot), \dots, f(\theta_K; \cdot)$
Algorithms : AL, GAL

$$\text{Residual}(F^{t-1}(\mathbf{X}), \mathbf{y}) = \begin{cases} \mathcal{L}(F^{t-1}(\mathbf{X}), \mathbf{y}) & , \text{AL} \\ \frac{\partial}{\partial F^{t-1}(\mathbf{X})} \mathcal{L}(F^{t-1}(\mathbf{X}), \mathbf{y}) & , \text{GAL} \end{cases}$$

$$\text{Merge}_{i=1}^k f(\theta_1^t; \mathbf{X}_1) = \begin{cases} \eta^t \sum_{i=1}^k f(\theta_i^t; \mathbf{X}_i) & , \text{AL} \\ \eta^t \sum_{i=1}^k w_i^t f(\theta_i^t; \mathbf{X}_i) & , \text{GAL} \end{cases}$$

```

1 Initialize  $\theta_1^0, \dots, \theta_K^0$ ; initialize  $F^0 \leftarrow 0$ ;
2 for  $t = 1, \dots, T$  do
3    $\mathbf{r}_1^t \leftarrow \text{Residual}(F^{t-1}(\mathbf{X}), \mathbf{y})$ ;                                /*  $P_1$ : Compute residual */
4   for  $i = 1, \dots, k$  do
5      $\theta_i^t \leftarrow \arg \min_{\theta_i^t} \mathcal{L}(f(\theta_i^t; \mathbf{X}_i), \mathbf{r}_1^t)$ ;                /*  $P_K$ : Optimize local model */
6    $F^t(\mathbf{X}) \leftarrow F^{t-1}(\mathbf{X}) + \text{Merge}_{i=1}^k f(\theta_i^t; \mathbf{X}_i)$ ;          /*  $P_1$  Update ensemble model */

```

B.2 Split-NN-based VFL Algorithms

As described in Algorithm 3, each iteration t starts with the parties P_i conducting forward-propagation on their local data \mathbf{X}_i to derive local representation \mathbf{Z}_i^t (line 4). These representations are subsequently forwarded to the primary party P_1 . Depending on the iteration, P_1 then merges the local

representations (line 6), further derives a global prediction $\hat{\mathbf{y}}^t$ with an aggregated model (line 7), updates the aggregated model parameters θ_1^t (line 8), and broadcast the encoded aggregation model θ_1^t to all parties (line 9). The parties P_i then employ these encoded aggregation model to update their local models (line 11). This process is repeated until a specified criterion for stopping is met.

The specific methods of encoding, determining aggregation frequency, and merging are dependent on the algorithm design. In the process of forward-pass encoding, SplitNN sends local representations directly to Party P_1 for merging, while C-VFL compresses these representations before transmission. In contrast, BlindFL utilizes a source layer to encode local representations, ensuring privacy preservation. During backward-pass encoding, C-VFL transmits the top-k-compressed aggregation model. Both SplitNN and BlindFL initially compute the gradients with respect to \mathbf{Z} and subsequently broadcast either the raw or source-layer encoded gradients to all the parties. Regarding aggregation frequency, C-VFL aggregates every Q iterations to reduce communication cost, while both SplitNN and BlindFL aggregate at every iteration. For the merging process, SplitNN and C-VFL use concatenation of local representations, while BlindFL applies a secret-sharing summation with source-layer-encoded representations.

Algorithm 3: Outline of split-NN-based VFL algorithms

Input : Number of iterations T ; number of parties K ; data and labels of primary party \mathbf{X}_1, \mathbf{y} , learning rate η^t ; data of secondary parties $\mathbf{X}_2, \dots, \mathbf{X}_K$; local epochs Q

Output : Models on K parties $f(\theta_1; \cdot), \dots, f(\theta_K; \cdot)$

Algorithms : SplitNN, C-VFL, BlindFL

$$\text{Encode}(\mathbf{Z}) = \begin{cases} \mathbf{Z} & , \text{SplitNN} \\ \text{EmbeddingCompress}(\mathbf{Z}) & , \text{C-VFL} \\ \text{SourceLayer}(\mathbf{Z}) & , \text{BlindFL} \end{cases}$$

$$\text{Encode}(\theta_1^t) = \begin{cases} \frac{\partial}{\partial \mathbf{Z}_1^t} \mathcal{L}(\hat{\mathbf{y}}^t, \mathbf{y}; \theta_1^t) & , \text{SplitNN} \\ \text{TopK}(\theta_1^t) & , \text{C-VFL} \\ \text{SourceLayer}(\frac{\partial}{\partial \mathbf{Z}_1^t} \mathcal{L}(\hat{\mathbf{y}}^t, \mathbf{y}; \theta_1^t)) & , \text{BlindFL} \end{cases}$$

$$\text{condition}(t) = \begin{cases} \text{True} & , \text{SplitNN, BlindFL} \\ t \bmod Q = 0 & , \text{C-VFL} \end{cases}$$

$$\text{Merge}_{i=1}^k \mathbf{Z}_i^t = \begin{cases} \text{Concatenate}(\mathbf{Z}^1, \dots, \mathbf{Z}^t) & , \text{SplitNN, C-VFL} \\ \text{SecretSharingSum}(\mathbf{Z}^1, \dots, \mathbf{Z}^t) & , \text{BlindFL} \end{cases}$$

```

1 Initialize  $\theta_1^0, \dots, \theta_K^0$ ;
2 for  $t = 1, \dots, T$  do
3   for  $i = 1, \dots, k$  do
4      $\mathbf{Z}_i^t \leftarrow \text{Encode}(f(\theta_i^t; \mathbf{X}_i))$ ;           /*  $P_i$ : Get local representations */
5   if condition( $t$ ) then
6      $\mathbf{Z}^t \leftarrow \text{Merge}_{i=1}^k \mathbf{Z}_i^t$ ;           /*  $P_1$ : Merge local representations */
7      $\hat{\mathbf{y}}^t \leftarrow f(\theta_1^t; \mathbf{Z}^t)$ ;           /*  $P_1$ : Get global prediction */
8      $\theta_1^t \leftarrow \theta_1^{t-1} - \eta^t \frac{\partial}{\partial \mathbf{Z}_1^t} \mathcal{L}(\hat{\mathbf{y}}^t, \mathbf{y})$ ; /*  $P_1$ : Update aggregated model */
9      $\mathbf{g}_i^t \leftarrow \text{Encode}(\theta_1^t)$ ;           /*  $P_1$ : Encode aggregated model */
10  for  $i = 1, \dots, k$  do
11     $\theta_i^t \leftarrow \theta_i^{t-1} - \eta^t \mathbf{g}_i^t$ ;           /*  $P_i$ : Update local model */

```

B.3 Split-GBDT-based VFL Algorithms

Outlined in Algorithm 4, each iteration t initiates with the primary party P_1 encoding the gradient of residuals, yielding \mathbf{r}^t (line 3). Following this, all parties P_i calculate local histograms \mathbf{H}_i^t utilizing their individual local data \mathbf{X}_i and the encoded residuals \mathbf{r}^t (line 5). These local histograms are then transmitted to P_1 for merging (line 6). In the next step, P_1 trains a decision tree using the merged histogram \mathbf{H}^t and the encoded residuals \mathbf{r}^t (line 7). The selected split points from this tree are communicated to the secondary party that possesses the split feature, which stores these split points

for potential future requests during inference (line 9). Finally, P_1 updates the ensemble model F^t with the newly trained tree (line 10). This sequence of operations continues until a set stopping condition is fulfilled.

Depending on the algorithm, the specific techniques for encoding, computing histograms, merging, and updating modes differ. Pivot views the instance set in each node as confidential information, implementing homomorphic encryption on it. Conversely, SecureBoost, FedTree, and VF2Boost treat the instance set as public information and apply homomorphic encryption only on a specific set of instances. In terms of merging, SecureBoost and FedTree perform homomorphic decryption directly to acquire actual sum values after aggregating encrypted histograms. VF2Boost further introduces efficiency measures such as Polynomial-based histogram packing and reordered histogram accumulation, while Pivot utilizes multi-party computation supporting comparison to maintain the secrecy of values at all times. In terms of the update mode, SecureBoost, Pivot, and FedTree adopt a sequential approach, whereas VF2Boost utilizes a pipeline processing for speedup. Additionally, it is worth mentioning that SecureBoost employs a threshold for binary classification to enhance accuracy in the context of datasets with label imbalance.

Algorithm 4: Outline of split-GBDT-based VFL algorithms

Input : Number of iterations T ; number of parties K ; data and labels of primary party \mathbf{X}_1, \mathbf{y} , learning rate η^t ; data of secondary parties $\mathbf{X}_2, \dots, \mathbf{X}_K$
Output : Models on K parties $f(\theta_1; \cdot), \dots, f(\theta_K; \cdot)$
Algorithms : SecureBoost, Pivot, FedTree, VF2Boost

HE = HomomorphicEncrypt, HD = HomomorphicDecrypt, MPC = MultiPartyComputationEncode, \otimes is homomorphic multiplication, α is instance mask

Encode(\mathbf{Z}) = $\begin{cases} \text{HE}(\mathbf{r} \cdot \alpha) & \text{, SecureBoost, FedTree, VF2Boost} \\ \mathbf{r} \otimes \text{HE}(\alpha) & \text{, Pivot} \end{cases}$

Hist(\mathbf{X}, \mathbf{r}) = $\begin{cases} \text{HE}(\text{Histogram}(\mathbf{X} \cdot \alpha, \mathbf{r})) & \text{, SecureBoost, FedTree, VF2Boost} \\ \text{Histogram}(\mathbf{X}, \mathbf{r}) \otimes \text{HE}(\alpha) & \text{, Pivot} \end{cases}$

Merge $_{i=1}^k \mathbf{H}_i^t = \begin{cases} \text{HD}(\text{HESum}(\mathbf{H}_1^t, \dots, \mathbf{H}_K^t)) & \text{, SecureBoost, FedTree} \\ \text{HD}(\text{Pack}(\text{HESum}(\text{Re-order}(\mathbf{H}_1^t, \dots, \mathbf{H}_K^t)))) & \text{, VF2Boost} \\ \text{MPC}(\text{HESum}(\mathbf{H}_1^t, \dots, \mathbf{H}_K^t)) & \text{, Pivot} \end{cases}$

mode = $\begin{cases} \text{sequence} & \text{, SecureBoost, Pivot, FedTree} \\ \text{pipeline} & \text{, VF2Boost} \end{cases}$

```

1 Initialize  $\theta_1^0, \dots, \theta_K^0$ ; let federated model  $F^0(\cdot) \leftarrow 0$ ;
2 for  $t = 1, \dots, T$  in mode do
3    $\mathbf{r}^t \leftarrow \text{Encode}(\frac{\partial}{\partial F^{t-1}} \mathcal{L}(F^{t-1}(\mathbf{H}^{t-1}), \mathbf{y}))$ ;          /*  $P_1$ : Encode gradients */
4   for  $i = 1, \dots, k$  do
5      $\mathbf{H}_i^t \leftarrow \text{Hist}(\mathbf{X}_i, \mathbf{r}^t)$ ;          /*  $P_i$ : Compute local histogram */
6    $\mathbf{H}^t \leftarrow \text{Merge}_{i=1}^k \mathbf{H}_i^t$ ;          /*  $P_1$ : Merge local histograms */
7    $\theta_1^t \leftarrow \arg \min_{\theta_1^t} \mathcal{L}(f(\theta_1^t; \mathbf{H}^t), \mathbf{r}^t)$ ;          /*  $P_1$ : Construct tree */
8   for  $i = 2, \dots, k$  do
9      $\theta_i^t \leftarrow \text{Selected split points in } \mathbf{H}_i^t$ ;          /*  $P_i$ : Update secondary parties */
10   $F^t(\mathbf{H}^t) \leftarrow F^{t-1}(\mathbf{H}^{t-1}) + f(\theta_1^t; \mathbf{H}^t)$ ;          /*  $P_1$ : Update ensemble model */

```

C Split Method Details

In this section, we formally state out proposed importance-based feature-split algorithm in Algorithm 5. After initializing local datasets for each party (line 1), a series of probabilities p_1, \dots, p_K s.t. $\sum_{i=1}^K p_i = 1$ is sampled from a Dirichlet distribution, parameterized by $\alpha_1, \dots, \alpha_K$ (line 2). For each feature, it then proceeds to randomly select a party P_k , according to the probabilities p_k , and assigns the respective feature to P_k (lines 3-5). In order to address potential failures in algorithms when confronted with empty features, we can optionally initialize each party with a random feature prior to the commencement of the algorithm.

Algorithm 5: Feature Splitting by Importance

Input: Global dataset $\mathbf{X} \in \mathbb{R}^{n \times m}$, importance factors $\alpha_1, \dots, \alpha_K$ **Output:** Local datasets $\mathbf{X}_1, \dots, \mathbf{X}_K$

```
1  $\mathbf{X}_1, \dots, \mathbf{X}_K \leftarrow \emptyset;$  /* Initialize local dataset for  $P_i$  */
2  $p_1, \dots, p_K \leftarrow \text{Dirichlet}(\alpha_1, \dots, \alpha_K);$  /* Sample probabilities for  $K$  parties */
3 for  $j = 1, \dots, m$  do
4    $k \leftarrow \text{Random choice from } [1, K] \cup \mathbb{N} \text{ w.p. } (p_1, \dots, p_K);$  /* Choose a party */
5    $D_k \leftarrow D_k \cup \{\mathbf{X}[:, j]\};$  /* Add feature  $\mathbf{X}[:, j]$  to  $P_k$  */
6 return  $\mathbf{X}_1, \dots, \mathbf{X}_K$ 
```

D Empirical Validation of Split Methods

To rigorously evaluate the practical performance of our proposed correlation evaluation metric and the correlation-based feature-split algorithm, we conduct a series of systematic experiments.

D.1 Correlation Evaluation Metric

In order to validate the efficacy of the correlation evaluation metric, Pcor, we create two synthetic datasets, \mathbf{X}_1 (m_1 features) and \mathbf{X}_2 (m_2 features), using the `sklearn` library. Initially, party P_1 holds \mathbf{X}_1 , and P_2 holds \mathbf{X}_2 . Over the course of the experiment, we gradually transfer features from \mathbf{X}_1 to P_2 , each time exchanging for a feature of \mathbf{X}_2 . This process continues until all features of \mathbf{X}_1 end up on P_2 , while the total number of features remains constant during the whole process.

Our observations, as presented in Figure 4a and 4b, reveal the following: (1) Pcor behaves similarly to mcor when evaluating inner-party correlation and shows a similar trend to mcor [34] when assessing inter-party correlation. (2) Both Pcor and mcor exhibit the lowest inter-party correlation and the highest inner-party correlation at the extremities of the x-axis. This suggests that the datasets \mathbf{X}_1 and \mathbf{X}_2 are managed by distinct parties and exhibit complete independence. This pattern is also reflected in Figure 4c when Pcor is applied to parties of different dimensions. These observations validate the appropriateness of Pcor as a measure for evaluating inter-party correlation, even when the number of features between the two parties varies.

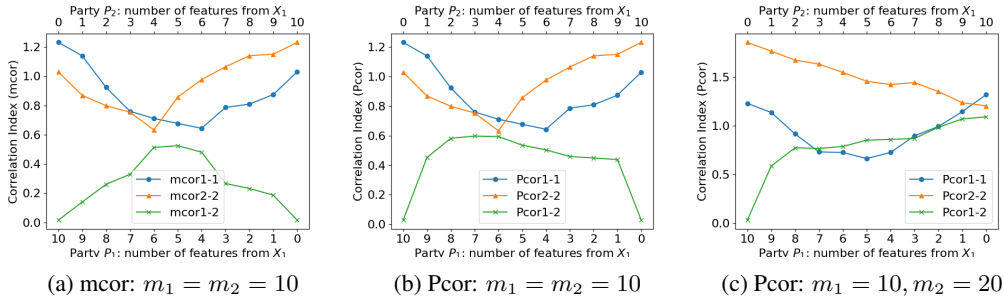


Figure 4: The trend of correlation and metrics when exchanging features between two parties. mcor: multi-way correlation [34]; Pcor(i)-(j): $\text{Pcor}(\mathbf{X}_i, \mathbf{X}_j)$; mcor(i)-(j): $\text{mcor}(\mathbf{X}_i, \mathbf{X}_j)$.

D.2 Correlation-based Feature-split Algorithm

We turn our attention towards validating the efficacy of our proposed correlation-based feature-split algorithm. Three synthetic datasets, each encompassing 10 features, are independently generated using the `sklearn` library. These datasets are subsequently concatenated along the feature axis, yielding a global dataset with 30 features. This dataset is then split into three local datasets, each containing 10 features, deploying our proposed algorithm with β values set at 0, 0.5, and 1.0.

The visualization of the absolute value of the correlation matrix between each pair of features is presented in Figure 5. As evident in Figure 5a, 5b, and 5c, an increment in the value of β corresponds to an increase in the correlation between features of different parties. This observation is in alignment

with our expectations. However, randomly splitting features into three parties, serving as our baseline, fails to reflect scenarios with low inter-party correlation (as illustrated in Figure 5d). These empirical findings underscore the efficacy of our proposed algorithm in partitioning features based on their correlation attributes.

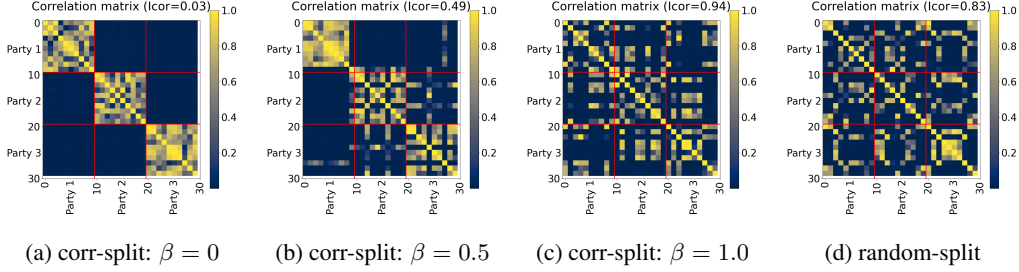


Figure 5: Correlation matrix of the global dataset with party boundaries indicated by red lines

D.3 Time Efficiency of Split Methods.

Table 3 provides a summary of the estimated time requirements for our proposed split methods, with the I/O time for loading and saving datasets excluded. Notably, the importance-based split method demonstrates significant efficiency, typically completing within a minute. In contrast, the correlation-based split method requires a longer processing time, due to the need to resolve three optimization problems. This time cost is especially pronounced on high-dimensional datasets, such as realsim, because the singular value decomposition (SVD) used in the correlation-based split algorithm is dependent on the number of features. Despite these differences in time consumption, both split methods prove capable of handling large datasets, accommodating instances up to 581k and features up to 20k, within a reasonable time frame.

Table 3: Estimated time cost of splitting methods (in seconds)

Dataset	Performance of importance-based split				Performance of correlation-based split			
	$\alpha = 0.1$	$\alpha = 1$	$\alpha = 10$	$\alpha = 100$	$\beta = 0$	$\beta = 0.3$	$\beta = 0.6$	$\beta = 1$
covtype	0.21	0.24	0.26	0.27	64.15	55.77	53.19	69.34
msd	0.29	0.27	0.29	0.30	85.39	68.88	64.76	62.01
gisette	0.23	0.29	0.25	0.27	6743.26	6388.56	5640.81	6733.69
realsim	30.11	29.80	30.60	26.68	13681.97	13381.56	11341.31	10057.42
letter	0.00	0.00	0.00	0.00	43.15	46.01	41.50	38.72
epsilon	12.67	12.30	10.36	12.28	4853.63	4395.76	4105.53	3621.99
radar	0.14	0.15	0.16	0.15	308.61	274.06	236.73	299.12

E Real Dataset Construction

In this section, we outline the construction process of the Satellite dataset, which was adapted from the WorldStrat dataset [63], originally intended for high-resolution imagery analysis. The Satellite dataset encompasses Point of Interest (POI) data, each associated with one or more Areas of Interest (AOI). Every AOI incorporates a unique location identifier, a land type, and 16 low-resolution, 13-channel images, each taken during a satellite visit to the location.

During the data cleaning phase, we scrutinize the dataset thoroughly, identifying and removing 67 incomplete data records that have an insufficient number of low-resolution images. Furthermore, given the inconsistent widths and heights of images across different locations, we standardize the size of all images to a 158x158 square via bicubic interpolation. Additionally, the pixel values of each image are scaled to integer values within the range of $[0, 255]$.

The Satellite dataset forms a practical VFL scenario for location identification based on satellite imagery. Each AOI, with its unique location identifier, is captured by 16 satellite visits. Assuming each visit is carried out by a distinct satellite organization, these organizations aim to collectively

train a model to classify the land type of the location without sharing original images. The Satellite dataset encompasses four land types as labels, namely Amnesty POI (4.8%), ASMSpotter (8.9%), Landcover (61.3%), and UNHCR (25.0%), making the task a 4-class classification problem of 3927 locations.

License. Our use of the WorldStrat dataset was restricted to the labels and Sentinel2 imagery, falling under the CC BY 4.0 [71] license, while excluding high-resolution imagery that falls under the CC BY-NC 4.0 [72] license. Therefore, we have released the Satellite dataset under the CC BY 4.0 license.

File description and maintenance plan. We aim to create a dedicated website for federated learning datasets to host the Satellite dataset and future VFL datasets. Although the website is currently under construction, we have made the Satellite dataset available via a public Google Drive link [73] for review purposes. The provided ZIP file comprises 32 CSV files, corresponding to training and testing datasets split at a ratio of 8:2. Each training and testing file contains 3,142 and 785 flattened images from a party, respectively.

F Experimental Details

Datasets. The datasets employed in our experiments exhibit a range of dimensions (from 16 to 20,958), instance numbers (from 15k to 581k), and tasks, which include binary classification, multi-class classification, and regression. Detailed information about these datasets and the corresponding licenses are presented in Table 4.

Table 4: Detailed information of datasets (N/A means unspecified)

Dataset	Task	#samples	#features	#classes	License
covtype [64]	classification	581,012	54	7	BSD [74]
msd [65]	regression	463,715	90	1	CC BY-NC-SA 2.0 [75]
gisette [66]	classification	60,000	5,000	2	CC BY 4.0 [71]
realsim [67]	classification	72,309	20,958	2	N/A
epsilon [68]	classification	400,000	2,000	2	N/A
letter [69]	classification	15,000	16	26	N/A
radar [70]	classification	325,834	174	7	N/A

Hyperparameters. For models based on split-GBDT, such as SecureBoost, FedTree, and Pivot, our experiments are conducted with the following hyperparameters: `learning_rate=0.1`, `num_trees=50`, `max_bin=32`, and `max_depth=6`. Due to the constraints of dataset sizes in their codes, Pivot is evaluated exclusively on two datasets: the letter dataset under the default setting of `MAX_GLOBAL_SPLIT_NUM=6,000` and on the gisette dataset with `MAX_GLOBAL_SPLIT_NUM=500,000`. The latter alteration was necessitated by a segmentation fault encountered under the default setting.

With regard to Split-NN-based models, specifically SplitNN and C-VFL, each local model is trained by a two-layer multi-layer perceptron (MLP) with each hidden layer containing 100 units. The corresponding aggregated model is a single-layer MLP with 200 hidden units. The learning rate, chosen from the set $\{10^{-4}, 10^{-3}, 3 \times 10^{-3}\}$, is contingent on the specific algorithm and dataset. The number of iterations is fixed at 50 for SplitNN and 200 for C-VFL, with the latter setting aimed at ensuring model convergence. We also test C-VFL using four quantization buckets, a single vector quantization dimension, and a top-k compressor as recommended in the default setting. The number of local rounds Q in C-VFL is set to 10.

Finally, for the ensemble-based model, GAL, we utilize a `learning_rate=0.01`, `local_epoch=20`, `global_epoch=20`, and `batch_size=512`, with the assist mode set to `stack`. In the GAL framework, each party employs an MLP model consisting of two hidden layers, each containing 100 hidden units.

Environments. The hardware configuration used for C-VFL, GAL, SplitNN, and FedTree consists of 2x AMD EPYC 7543 32-Core Processors, 4x A100 GPUs, and 503.4 GB of RAM, running

on Python 3.10.11 with PyTorch 2.0.0, Linux 5.15.0-71-generic, Ubuntu 22.04.2 LTS. For FATE framework, we are using `federatedai/standalone_fate` Docker image, running with Python 3.8.13 on Docker 23.0.2. Pivot is compiled from source using CMake 3.19.7, g++ 9.5.0, libboost 1.71.0, libscapi with git commit hash 1f70a88, and runs on a slurm cluster with AMD EPYC 7V13 64-Core Processor with the same number of cores as 2x AMD EPYC 7543 used for other algorithms.

License. The licenses pertinent to the datasets and algorithms utilized in VertiBench are documented in Table 4 and Table 5, respectively. We ensure adherence to these licenses as VertiBench neither redistributes the codes and data nor utilizes them for any commercial purpose.

Table 5: License usage for each VFL algorithm.

Algorithm	License	Share	Commercial use	Redistribute
GAL [5]	MIT [76]	✓	✓	✓
C-VFL [21]	MIT [76]	✓	✓	✓
SecureBoost [22]	Apache 2.0 [77]	✓	✓	✓
Pivot [52]	CC BY-NC-ND 4.0 [78]	✓	✗	✗
FedTree [29]	Apache 2.0 [77]	✓	✓	✓

Note: AL [6], SplitNN [7], BlindFL [50] and VF2Boost [55] do not specify their licensing terms.

G Additional Experiments

G.1 Communication Cost Details

In this subsection, we analyze the maximum incoming and outgoing communication of each VFL algorithm (Figure 6), which aligns with our observations in Section 6.3.

Generally, GAL is more efficient than FedTree, albeit FedTree has less incoming communication cost on low-dimensional datasets. The incoming communication cost includes residuals for GAL and histograms for FedTree. Residual size is dependent on the number of instances, while histogram size relates to the feature count. Hence, FedTree shows less incoming communication cost on low-dimensional datasets but more on high-dimensional datasets. However, FedTree’s outgoing communication cost is approximately twice that of GAL, as it transmits both gradients and Hessians, neutralizing its incoming communication efficiency on low-dimensional datasets.

C-VFL primarily reduces communication costs via representation compression sent to the server, yet it does not enhance the backward server-client communication. This substantial reduction in the incoming communication cost is indicative of a noteworthy decrease in the representation size. Conversely, the consistent outgoing communication cost suggests that the transmission of compressed aggregated models within C-VFL is not demonstrating greater efficiency compared to the process of transmitting uncompressed gradients of the cut layer. Such an observation provides insights into potential enhancements that could be pursued to reduce SplitNN’s backward communication costs.

G.2 Scalability

In this section, we examine the scalability of various VFL algorithms on two high-dimensional datasets, depicted in Figure 7. The datasets, split by importance with $\alpha = 1$, consist of a varying number of parties, ranging from 2 to 2048. Our results demonstrate that **SplitNN and FedTree are scalable to thousands of parties without any significant drop in accuracy**. This is attributable to FedTree’s lossless design and SplitNN’s robust structure. However, both GAL and C-VFL show substantial performance declines with an increase in party numbers.

An intriguing observation is that **C-VFL’s accuracy nearly matches SplitNN’s when the number of parties reaches 2048 on the gisette dataset**. This is likely because the average number of features per party reduces to 2 in this scenario, causing the compression mechanism to potentially fail, and thus, C-VFL reverts to SplitNN’s performance.

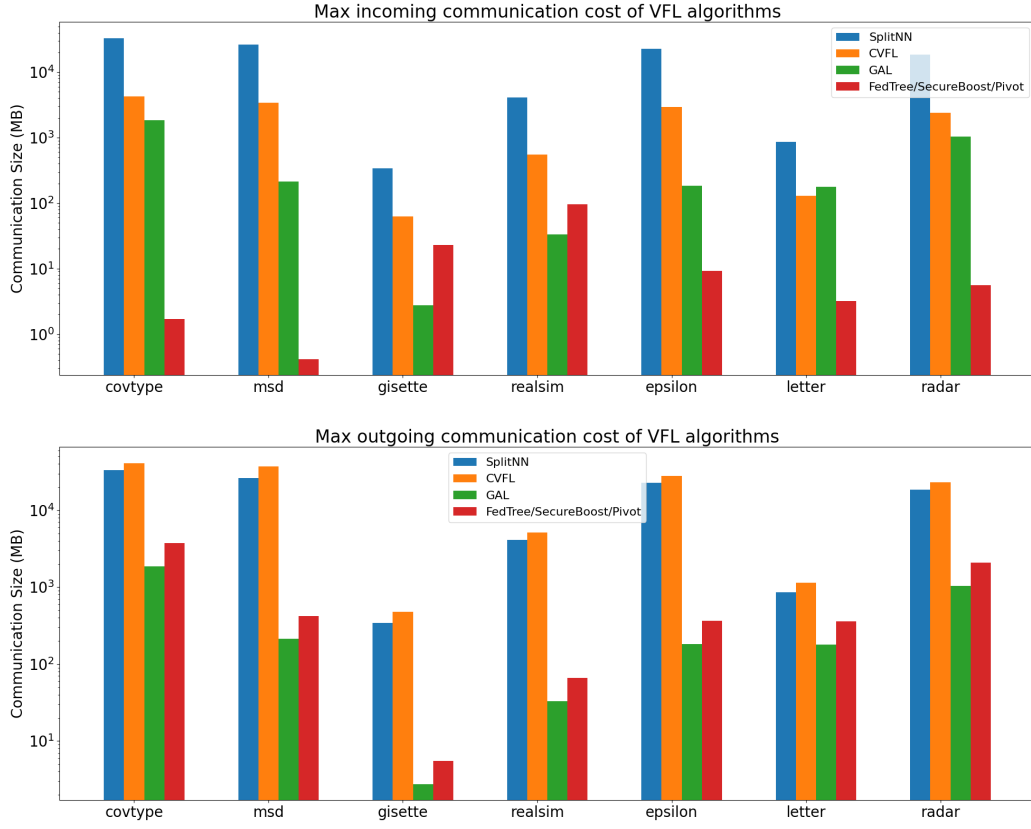


Figure 6: The max incoming and outgoing communication size of VFL algorithms (50 global iterations)

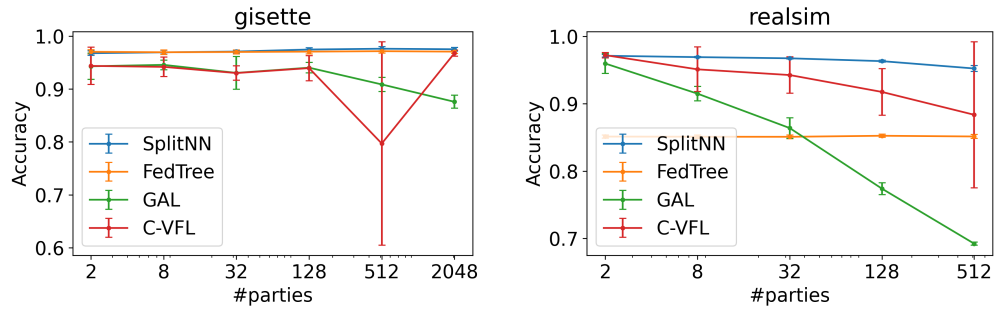


Figure 7: Scalability tests for VFL algorithms on gisette and realsim dataset

G.3 Training Time

The training duration for VFL algorithms is consolidated in Table 6. It should be noted that FedTree and SecureBoost are executed without the use of encryption or noise. Conversely, we retain the default privacy setting for Pivot as it does not offer a non-encryption alternative. Three observations can be gleaned from the table.

Firstly, **we observe a considerable overhead associated with the encryption processes of Pivot**. Pivot, which employs both homomorphic encryption and secure multi-party computation to ensure stringent privacy, endures a training time that is up to 10^5 times longer than FedTree. This limitation renders such strict privacy measures impractical for real-world applications that employ large datasets. This observation underscores the necessity for further exploration into the efficiency-privacy trade-off in VFL.

Secondly, when comparing non-encryption methods, we find that **split-based algorithms (SplitNN, FedTree) generally outperform ensemble-based algorithms (GAL) in terms of efficiency**. This is primarily because split-based algorithms require each party to train a partial model, whereas ensemble-based algorithms mandate that each party train an entire model for ensemble purposes. This design characteristic also contributes to the lower communication costs associated with ensemble-based algorithms, as demonstrated in Figure 3 and Figure 6.

Lastly, we note that **SplitNN demonstrates higher efficiency than FedTree on high-dimensional small datasets, yet demands more training time on low-dimensional large datasets**. This discrepancy arises because FedTree computes a fixed-size histogram for each feature, which alleviates the impact of a large number of instances but is sensitive to the number of features. Conversely, SplitNN trains data in batches, rendering it sensitive to the number of instances. This observation emphasizes the importance of carefully selecting a VFL algorithm based on the properties of the dataset in the application.

Table 6: Estimated training time of VFL algorithms (4-party, in hours)

Dataset	VFL Algorithm					
	SplitNN	GAL	FedTree	SecureBoost	C-VFL	Pivot ¹
covtype	0.19	2.18	0.076	14.84	1.45	-
msd	0.17	2.01	0.037	0.28	1.29	-
gisette	0.01	0.03	0.052	0.56	0.02	25805.52
realsim	0.06	1.40	0.32	1.16	0.48	-
epsilon	0.15	1.79	0.33	7.99	1.11	-
letter	0.01	0.06	0.47	2.69	0.04	6750.76
radar	0.12	1.31	0.21	10.06	0.83	-

¹ A segmentation fault arises in Pivot when datasets encompass more than 60,000 samples. Consequently, only the gisette and letter datasets have their training times estimated.

G.4 Performance on Satellite dataset

In Table 7, we present the single-party and VFL performance results on the Satellite dataset. For an equitable comparison, each single party trains a concatenated MLP, formed by linking a SplitNN’s local model with its aggregated model, under the same hyperparameters. Our results indicate that VFL can yield approximately a 10% accuracy improvement over local training, thus affirming the practical utility of the Satellite dataset for vertical federated learning applications.

H Discussion

This section discusses the limitations of VertiBench, shedding light on several areas where improvement is needed. Additionally, we engage in a discussion surrounding potential negative social impacts and personal privacy issues related to VertiBench.

Table 7: Accuracy of single party training (Solo) and VFL with SplitNN on Satellite dataset

Method	Accuracy (mean \pm standard deviation)
Party P_0 (Solo)	0.7368 ± 0.0086
Party P_1 (Solo)	0.7310 ± 0.0054
Party P_2 (Solo)	0.7320 ± 0.0055
Party P_3 (Solo)	0.7289 ± 0.0115
Party P_4 (Solo)	0.7251 ± 0.0080
Party P_5 (Solo)	0.7167 ± 0.0097
Party P_6 (Solo)	0.7353 ± 0.0045
Party P_7 (Solo)	0.7256 ± 0.0139
Party P_8 (Solo)	0.7335 ± 0.0126
Party P_9 (Solo)	0.7154 ± 0.0049
Party P_{10} (Solo)	0.7264 ± 0.0172
Party P_{11} (Solo)	0.7169 ± 0.0106
Party P_{12} (Solo)	0.7182 ± 0.0075
Party P_{13} (Solo)	0.7118 ± 0.0084
Party P_{14} (Solo)	0.7060 ± 0.0119
Party P_{15} (Solo)	0.7292 ± 0.0069
Party $P_1 \sim P_{15}$ (SplitNN)	0.8117 ± 0.0035

H.1 Limitations

In this subsection, we outline the limitations of VertiBench, focusing on three primary aspects.

Scalability of correlation-based split. The correlation-based split method that we propose may face efficacy and efficiency challenges when applied to a large number of parties. As the number of parties increases, the potential feature splits proliferate exponentially. This complexity presents a significant obstacle for optimization methods such as BRKGA [60], making it challenging to locate the minimum and maximum Icor, as well as the optimal split that corresponds to the given β . This situation underscores the necessity for more advanced permutation-based optimization algorithms that can enable the correlation-based split method to scale out to a greater number of parties.

Relationship between importance and correlation. Within VertiBench, we regard importance and correlation as two orthogonal factors impacting the feature split. However, this viewpoint might overlook the potential correlation that could exist between these two factors. For instance, in cases of highly imbalanced feature split, parties might demonstrate low inter-party correlation. As a result, a comprehensive benchmarking framework that simultaneously considers both importance and correlation is desired to provide a more rigorous evaluation of VFL algorithms.

Evaluation of privacy. Although VertiBench assesses performance, efficiency, and communication cost, it does not provide a quantitative evaluation of privacy. The high performance observed with SplitNN could potentially come at the cost of privacy, while the markedly high overhead of Pivot might be attributed to its robust privacy requirements. The task of quantitatively evaluating the privacy of different VFL algorithms and models remains an open problem, which we aim to tackle in future work.

H.2 Social Impacts

Negative social impact. While VertiBench primarily focuses on analyzing and comparing existing methodologies, and hence is less likely to cause additional negative social impact, the potential for biased interpretation of our experimental results could inadvertently mislead future research or applications. Specifically, we emphasize that the superior performance of non-encrypted methods such as SplitNN and GAL does not necessarily indicate that they are fit for immediate deployment in real-world VFL applications. The privacy concerns arising from the transfer of residuals or representations require further investigations. A quantitative benchmark on privacy is a critical prerequisite to deploying VFL approaches in real-world applications, which we plan to explore in the future research.

Personal privacy. For synthetic datasets, VertiBench does not create new datasets but instead employs novel methods to split existing publicly available datasets, thereby avoiding any additional personal privacy issues. As for real-world data, our Satellite dataset pertains to land type data derived from the WorldStrat dataset, which does not contain personal information. The privacy protections implemented in the Satellite dataset align with those of the WorldStrat dataset, which asserts that direct or indirect identification of individuals is not possible [63]. In our approach, the use of low-resolution imagery in the Satellite dataset serves to further diminish any potential, albeit extremely unlikely, risk of accidentally capturing identifiable information about individuals. Consequently, we confidently assert that VertiBench does not pose any concerns regarding personal privacy.